universität wien

MASTERARBEIT / MASTER'S THESIS

Titel der Masterarbeit / Title of the Master's Thesis

„Evaluating DOM utilization patterns of marine deep-sea heterotrophic prokaryotes in the Southern Ocean using click-CARD-FISH and MICRO-CARD-FISH"

verfasst von / submitted by

Julia Steiger, BSc

angestrebter akademischer Grad / in partial fulfilment of the requirements for the degree of

Master of Science (MSc)

Wien, 2020 / Vienna, 2020

Studienkennzahl lt. Studienblatt / degree programme code as it appears on the student record sheet:	A 066 833
Studienrichtung lt. Studienblatt / degree programme as it appears on the student record sheet:	Masterstudium Ecology and Ecosystems
Betreut von / Supervisor:	Univ.-Prof. Dr. Gerhard J. Herndl

Acknowledgements

I would like to thank the captain and crew of the RV *Marion Dufresne* for their help during the research cruise and Ingrid Obernosterer for organizing it. Eva Sintes conducted microautoradiography and click work at sea and provided the results of liquid scintillation counter measurements. This study, principally supervised by Eva Sintes and Gerhard J. Herndl, was supported by the Austrian Science Fund (FWF; P27696-B22) to ES and by the Austrian Science Fund (FWF) project ARTEMIS (P 28781-B21) to GJH. I also want to thank all the members of the MOVie group for their support and for creating such a nice working atmosphere. Special thanks are directed to my colleagues of the Masters' office for all the inspiring, exciting and fun moments during my work. Eva Sintes and Chie Amano are acknowledged for their advice, comments and great help during the whole project. Chie Amano always gave me a helping hand and guided me excellent through laboratory work and data analysis. Many thanks to Gerhard J. Herndl for giving me the chance to be part of his team. I appreciate all the experience I gained during my work under his supervision, especially in the constructive department meetings.

Abstract

Marine prokaryotes are key players in biogeochemical cycles. A key parameter to determine the contribution of specific prokaryotic taxa or cells to these cycles, as well as their ecological function, is the growth or activity rate. Several methods have been used to measure prokaryotic metabolic activity and biomass production by individual marine prokaryotic cells. Microautoradiography has been extensively used to detect substrate utilization by marine microbial cells for the past 20 years. Recently, 'click-chemistry' has been applied to detect the incorporation of fluorescently labeled amino acids into newly synthesized prokaryotic proteins. In this study we tested the applicability of click-chemistry to deep-sea samples, using L-homopropargylglycine (HPG), a methionine analog, and compared it to microautoradiography using tritium-labeled methionine. In addition, substrate uptake rates of Bacteria and Thaumarchaeota were compared by combining each of the two methods with catalyzed reporter deposition fluorescence in situ hybridization (CARD-FISH). Up to 55% of the total prokaryotic community took up methionine in the epipelagic waters of the Southern Ocean. A decreasing contribution of cells taking up methionine to the total prokaryotic cells from 100 m depth to 500 m depth was observed at the iron-limited sampling site. In contrast, the naturally iron fertilized sampling site exhibited a steady contribution of cells taking up methionine throughout the depth profile. Among the prokaryotic groups, bacteria were the major contributor to the prokaryotic cells taking up methionine, whereas only few Thaumarchaeota cells incorporated methionine. The click-CARD-FISH detected fewer active cells than the MICRO-CARD-FISH. However, our results indicate that both methods reveal similar substrate utilization patterns of marine prokaryotic communities throughout the water column.

Introduction

Marine prokaryotes (Bacteria and Archaea) are key to global biogeochemical cycles, particularly to the carbon, nitrogen, phosphorous and sulfur cycle [1, 2]. Heterotrophic prokaryotes utilize organic matter released by autotrophs or other organisms to build up biomass and to gain energy [2, 3]. Incorporation of labeled compounds (e.g. labeled amino acids) into prokaryotic cells is an extensively used method to measure heterotrophic prokaryotic biomass production in aquatic systems [4]. However, the marine heterotrophic prokaryotic community consists of diverse taxa that varies in abundances and metabolic activity through space and time [5–10]. Consequently, the relative contribution of the individual taxa to the carbon flux is crucial to understand the function of marine ecosystems. Different methods have been developed to measure metabolic activity or *de novo* protein synthesis on a single-cell level, e.g. ion mass spectrometry [11–18] or Raman microspectroscopy [19–21] of isotopically labeled substrates (^{15}N-labeled ammonia or ^{13}C/^{15}N-labelled amino acids). These methods are either expensive, time consuming and/or require special devices and expertise. A frequently used method to assess single-cell protein synthesis by heterotrophic prokaryotes is microautoradiography. Microautoradiography is based on the incorporation of a radioisotope labeled substrate into macromolecules, followed by exposure to a photographic emulsion [22–24]. Since proteins constitute about half of the biomass of prokaryotic cells [4], radiolabeled amino acids, such as leucine (Leu) or methionine (Met) incorporation into newly synthesized proteins has been extensively used [25–28]. Radioisotope labeled thymidine (Thy) can be used to detect DNA synthesizing cells [29, 30]. Fluorescence *in* situ hybridization (FISH) allows determining the abundance of specific prokaryotic taxa by binding of fluorescently labeled oligonucleotide probes to target 16S rRNA [31, 32]. The oligonucleotide probes can also be labeled with horseradish peroxidase (HRP) to increase the sensitivity using catalyzed reporter deposition FISH (CARD-FISH) [33, 34]. Microautoradiography can be combined with the catalyzed reporter deposition fluorescence *in situ* hybridization (MICRO-CARD-FISH) [26] to identify the taxa taking up specific substrates and quantify single-cell uptake rates [27]. However, MICRO-CARD-FISH requires handling of radioactive substances. Consequently, it is expensive and implicate limitations, according to specific country or research vessel regulations, as well as the requirement of specialized personnel.

To overcome these problems involved in working with radioisotopes, fluorescently labeled biorthogonal non-canonical amino acid tagging (BONCAT) was recently applied to detect newly synthesized proteins in environmental samples [35–38]. Amino acid analogs, such as azidohomoalanine (AHA) [39–42] and homopropargylglycine (HPG) [37, 43] analogs of

methionine are incorporated into the polypeptide chain of proteins of natural prokaryotic assemblages. Subsequently, implementation of click chemistry results in fluorescent labeling of the cells that incorporated the analog. An analog of the nucleic acid thymidine that can be used to detect newly synthesized bacterial DNA in combination with click chemistry is 5-ethynyl-2'-deoxyuridine (EdU) [44]. The method can be coupled with catalyzed reporter deposition fluorescence in situ hybridization (click-CARD-FISH) to link phylogeny and activity [35, 36, 38]. Its applicability to microbial environmental samples has been shown for pond waters, anoxic sediments [36] coastal seawater [35, 37, 44], offshore shallow water samples [37] and deep-sea methane seep sediments [38].

In this study, bacterial and thaumarchaeal heterotrophic activity was determined with click-CARD-FISH and MICRO-CARD-FISH in Southern Ocean microbial communities. We addressed (I) the comparability of the bulk activity measurements obtained with click-CARD-FISH and MICRO-CARD-FISH, (II) the comparability of single-cell activity rates based on the quantification of the fluorescing area associated to click-CARD-FISH *vs*. the halo area around cells obtained by MICRO-CARD-FISH, (III) single-cell substrate uptake rate patterns of heterotrophic Bacteria and Thaumarchaeota throughout the water column in the Southern Ocean. Additionally, bulk uptake rates of radiolabeled methionine and thymidine by the bulk microbial community were determined.

Material and Methods

Study area and sampling. Samples for experiments were collected during the Mobydick cruise in the Southern Ocean close to the Kerguelen Islands onboard RV *Marion Dufresne* in March 2018. Water was collected with a CTD rosette sampler at the Kerguelen Plateau at Station M2 (72°01.34'E, 50°62.52'S) on 6 March down to 500 m depth and at Station M4 (67°19.26'E, 52°60.32'N) on 13 March down to 4000 m depth (Fig. 1). These two stations are characterized by contrasting environmental conditions; Station M2 is characterized by fairly high primary production associated to the naturally iron-fertilized waters, whereas Station M4 is a low primary productivity site, characterized by high nutrient and low chlorophyll *a* concentrations due to iron limitation [45–48].

Prokaryotic bulk uptake rates. Bulk uptake rates of methionine and thymidine by the prokaryotic community were determined by measuring the incorporation of ^{3}H-methionine and ^{3}H-thymidine into prokaryotic cells. Samples (10 – 40 mL; two live and one killed control per

depth) were inoculated with ^{3}H-methionine (final concentration, 20 nM; specific activity, 80 Ci mmol^{-1}; American Radiolabeled Chemicals, Inc.) or ^{3}H-thymidine (final concentration, 20 nM; specific activity, 71.7 Ci mmol^{-1}; Hartmann Analytic) and incubated in the dark at in situ temperature for 5 – 48 h, depending on the expected prokaryotic activity and abundance. The control was fixed with 0.2 µm-filtered formaldehyde (2% final concentration) prior to the addition of the radiolabeled substrate. The incubation was terminated by adding 0.2 µm-filtered formaldehyde (2% final concentration) to the live samples. Subsequently, the samples were filtered onto 0.2 µm polycarbonate filters, rinsed three times with 10 ml of 5% ice-cold trichloroacetic acid, transferred into scintillation vials and dried at room temperature. Thereafter, 8 mL of scintillation cocktail (FilterCount; Canberra Packard) was added to the vials. After 18 h, samples were counted with a liquid scintillation counter (Tri-Carb® 2100 TR, Perkin Elmer) and the obtained disintegrations per minute (dpm) were converted to methionine and thymidine incorporation rates (pmol L^{-1} h^{-1}) using the formula:

$$\text{Met (or Thy) incorporation (pmol L}^{-1}\text{ h}^{-1}\text{)} = [(dpm_L - dpm_C) / (t * 2.22\ 10^{12} * SA * V)] * 10^9$$

where, dpm_L is the average dpms on live samples, dpm_C is the dpms in the killed control, t is the incubation time in h, 2.22 x 10^{12} converts the radioactivity (dpm) to Ci, SA is the specific activity in Ci mmol^{-1}, and V is the sample volume in L.

Click-CARD-FISH and MICRO-CARD-FISH. Samples for click- and MICRO-CARD-FISH were processed immediately after collection. Different sample volumes (10 – 40 mL) and incubation times (5 – 48 h) were used depending on the expected prokaryotic abundance and activity. One live sample (TF) and one killed control (T0) were prepared for both methods (Click-CARD-FISH and MICRO-CARD-FISH). In order to save radiolabeled substrate, only one killed control for MICRO-CARD-FISH was used per depth profile.

Seawater samples were amended with the corresponding substrate: HPG (20 nM final concentration) for click-CARD-FISH and ^{3}H-Methionine (20 nM final concentration) and ^{3}H-Thymidine (20 nM final concentration) for MICRO-CARD-FISH. Killed controls were fixed with 0.2 µm-filtered formaldehyde (2% final concentration) 10 min prior to substrate addition. All live samples and controls were incubated in the dark at in situ temperature. The incubation was terminated by adding 0.2 µm-filtered formaldehyde (final conc. 2%). Subsequently, fixed samples were stored in the dark at 4°C for 12 – 24 h. Thereafter, samples were filtered onto 0.2 µm pore-size polycarbonate filter supported by a Millipore HA filter (0.45 µm pore size). The

filter was rinsed twice with 5 mL Milli-Q water, air dried and stored in 2 mL Eppendorf microfuge vials at -20°C until further processing at the home lab.

Click-CARD-FISH

(1) **Click-it reaction.** Chemicals to prepare the click-it reaction buffer (Supplementary Table S1) were thawed and subsequently kept on ice until mixing. The click reaction buffer was prepared in an Eppendorf microfuge vial. Light exposure was kept to a minimum throughout the click-CARD-FISH process to avoid damaging the fluorophore. Filters were labeled on the outer rim with a lead-pencil and placed on a glass slide to excise two triangular filter-pieces (~1/12 of the filter, one for enumerating Bacteria and one for enumerating Thaumarchaeota). The filter pieces were incubated in the click-it reaction buffer at room temperature in the dark for 30 min, and afterwards washed three times with Milli-Q water for 1 min. Subsequently, filter pieces were dried in light-protected petri dishes on a blotting paper in the hybridization oven at 37°C for 10 min.

(2) **CARD-FISH**

(2.1) **Embedding.** Filter pieces were embedded in warm low melting point agarose (0.1% w/v in Milli-Q water). The filter pieces were placed upside down on 5 µL agarose 0.1% drops deposited in an open petri dish, and dried at 37°C in the hybridization oven for 10-15 min. Afterwards, 96% ethanol (EtOH) was poured into the petri dish to facilitate the removal of the filters, which subsequently were air-dried.

(2.2) **Permeabilization.** For enumerating Bacteria, dried filter pieces were incubated in 10 mL lysozyme permeabilization mix (Table S2) in the hybridization oven in a petri dish in the dark at 37°C for 1 h. Thaumarchaeal cells were permeabilized in 0.1 M HCl in the dark at room temperature for 5 min. After permeabilization, filters for Bacteria and Thaumarchaeota were washed once and three times with Milli-Q water, respectively. Filter pieces were submerged in 0.01 M HCl in the dark at room temperature for 20-25 min, washed again twice with Milli-Q water, dipped shortly into 96% EtOH and dried.

(2.3) **Hybridization.** Bacteria were hybridized using 55% formamide hybridization buffer plus HRP labeled oligonucleotide probes: EUB338I, EUB338II, EUB338III [32, 49] (Table S3). Thaumarchaeota were hybridized using 20 % formamide hybridization buffer and a HRP labeled oligonucleotide probe mixture (CREN 554, CREN 537) [32, 44] (Table S3). Hybridization was performed in 0.6 mL Eppendorf microfuge vials wrapped in aluminum foil to avoid light exposure, slowly rotating in the hybridization oven at 35°C for 15 h.

(2.4) **Washing.** After hybridization, the filter sections were quickly transferred into the respective washing buffer (Table S4) and incubated in a water bath at 37°C for 15 min. Washing buffers were pre-warmed in the water bath at 37°C for 15-30 min.

(2.5) **Amplification.** Thereafter, the filters were incubated in 25 mL PBS-T mix (Table S5) at room temperature in the dark for 15 min, dried on blotting paper and placed in a 1.6 mL Eppendorf microfuge vial together with amplification buffer (Table S6). Amplification was performed in the hybridization oven at 46°C for 15 min. Thereafter, the excess amplification buffer was gently removed from the filters with a tissue paper. Next, filters were submerged in PBS-T mix at room temperature in the dark for 15 min. Then, filter sections were washed three times in Milli-Q water, dipped shortly into 96% EtOH and dried.

(3) **Internal standard fluorescence signal.** Fluorescing synthetic beads (0.3% intensity, mixed with Sigma water 1/10) were added to the filter sections as internal fluorescence standard. To prevent beads from aggregation during storage, the bead stock solution was vortexed shortly, sonicated for 10 min and vortexed shortly again prior to pipetting. For each filter section, 5 µL bead stock solution was pipetted onto a cover slip. The filter sections were placed onto the drop with the sample-side down and dried in the hybridization oven at 37°C for 10-15 min. Subsequently, filter sections were peeled off gently.

(4) **Cell transfer.** Filter-pieces were glued onto a TOMO object slide with wood glue mixed with Milli-Q water (0.5 polyvinyl acetate glue: 1 Milli-Q water) to transfer the cells from the filter onto the object slide. Cell transfer reduces the background fluorescence caused by the filter. Two separate 1 µL drops of glue for each filter section were placed on the object slide. The two drops were placed separated by the length of the filter section, and afterwards the glue was spread drawing a triangle shape of similar area to the filter-piece. Subsequently, the filter section was placed on the glue sample-side down. Thereafter, the slide was placed in a box containing silica gel and dried overnight at 4°C.

(5) **Peeling off the filter sections.** Before peeling off the filter, the shape of the filters was marked on the opposite side of the glass slide with a permanent marker. The filters were very gently and slowly peeled off with forceps so that the cells remained on the slide. Slight wetting of the filter outer rim (without cells) with a Milli Q-moistened tip facilitates the peeling. Afterwards cells were counterstained with DAPI mix (Table S7) and covered with a cover slip.

(6) **Microscopy and image analysis.** Slides were examined under the epifluorescence microscope (Zeiss; Axio, Imager.M2) equipped with filter sets for DAPI (DAPI channel; all cells), Alexa 488 (FITC channel; activity signal) and Alexa 555 (rhodamine channel, probe positive signal). A digital camera (AxioCam MRm, Carl Zeiss) was used to acquire pictures

using AxioVision software [www.zeiss.com/microscopy/int/products/microscope-software/axiovision.html]. At least 10 fields of view (FOV) and 1000 cells were evaluated per sample.

Three pictures (DAPI channel, FITC channel and rhodamine channel) from each field of view were taken and overlaid, with constant exposure time for FITC (2000 ms). The images were evaluated with ACMEtool2 [http://www.technobiology.ch/index.php?id=acmetool]. Killed controls were used to adjust the "set definitions" of ACMEtool2 used to set and subsequently correct for the background fluorescence in live samples.

Cells stained with DAPI represent the total abundance of prokaryotic cells. DAPI stained cells with overlapping signal in the FITC channel indicate HPG assimilating cells (active cells). DAPI stained cells with overlapping signal in the rhodamine channel represent either Bacteria or Thaumarchaeota cells.

(7) **Calculations**

(7.1) **Determination of active prokaryotic cells and of the activity of specific taxa.** The active cells as a percentage of the total DAPI stained cells was calculated by dividing the number of DAPI stained cells with overlapping signal in the FITC channel (incorporating HPG) by the total DAPI stained cells, multiplied by 100.

The percent of active cells of specific taxa was calculated by dividing the number of DAPI stained cells with an overlapping signal in the FITC channel (incorporating HPG) and the rhodamine channel (either Bacteria or Thaumarchaeota) by the DAPI stained cells with an overlapping signal in the rhodamine channel (either Bacteria or Thaumarchaeota), multiplied by 100.

(7.2) **Quantification of single cell activity.** The fluorescing area of the individual cells associated to the FITC channel (tentatively the HPG assimilating activity signal) is a proxy for cellular activity. The fluorescing area size (µm² MGV) was calculated by multiplying the intensity of the fluorescing signal (Mean grey value, MGV, output data of ACMEtool2) by the area of the fluorescing signal. The area size of each cell obtained from ACMEtool2 ($pixel^2$) was converted to μm^2 using a specific factor for the microscope magnification.

(I) Single cell uptake rates. The fluorescing area (see above) of each cell was divided by the incubation time in h (µm² MGV $cell^{-1}$ h^{-1}).

(II) Total uptake rates were calculated as the average of the total fluorescing area of the two evaluated filter pieces of a specific sample per liter and per hour (µm² MGV L^{-1} h^{-1}). The total fluorescing area (µm² MGV L^{-1} h^{-1}) of one filter was calculated using the following formula:

Total fluorescing area size (μm^2 MGV L^{-1} h^{-1}) = [(Σ of the fluorescing area of all counted cells of the filter / area of filter examined) x (total filtered area)] /(t x RR x V) x 1000

Where t is the incubation time in h, RR is the ratio of recovery (see below), and V is the sample volume in mL.

The ratio of recovery (RR) by click-CARD-FISH of DAPI-stained cells was calculated as follows:

RR = CCc / CCd

Where CCc is the average cell count per field of view obtained with the click-CARD-FISH and CCd is the average cell count per field of view obtained by direct DAPI staining (see below prokaryotic abundance evaluation).

MICRO-CARD-FISH

(1) **CARD-FISH.** CARD-FISH was performed as described above for click-CARD-FISH, with slight modifications. Permeabilization of Archaea was conducted in 0.1M HCl for 1 min. Amplification was done with the fluorophore Alexa 488, and blocking reagent concentration was 0.1% for both Bacteria and Archaea cells (Table S6). Filter-sections were washed twice with Milli-Q after the second PBS-T mix wash.

(2) **Microautoradiography.** The microautoradiography protocol has been previously described [26]. Coating of glass slides with the photographic emulsion (Ilford Nuclear Emulsion Type K5 and Sigma water 1:1 (v/v)) and transfer of the hybridized filter-sections into the emulsion were done under complete darkness. The slides were developed at 4°C for 4 d (when silver grain halo area did not further increase). Developing and fixing were performed according to the manufacturer's specifications using Ilford Developer (ILFORD PHENISOL) and Ilford Fixer (ILFORD HYPAM). Thereafter, the slides with the filters were air-dried in the dark for about 30 min.

(3) **Peeling off the filter-sections.** Filters were peeled off the glass slide and counterstained with the DAPI mix as described for click-CARD-FISH.

(4) **Microscopy and image analysis.** Microscopy and image analysis were conducted as described above. Appropriate filters for DAPI (DAPI channel, all cells) and for Alexa 488 (FITC channel, probe positive signal) were used. The transmission mode was used to detect silver grains (activity signal) associated with cells. The exposure time for transmission light was between 60 ms and 110 ms. Three pictures (DAPI channel, FITC channel and transmission channel) were acquired from each field of view, overlaid and evaluated with Axio Vision SE64 Re4.9 software (Carl Zeiss). DAPI positive cells with overlapping signal in the FITC channel identified either Bacteria or Thaumarchaeota. DAPI positive cells with

overlapping silver grain area in the transmission channel indicated methionine (Met) or thymidine (Thy) assimilating cells (activity signal, depending on the substrate added).

(5) **Calculations**

(5.1) **Determination of active prokaryotic cells and of the activity of specific taxa.** The contribution of active cells to the total community cells (in %) was calculated as the number of substrate incorporating cells (cells with associated silver grains), divided by the number of all DAPI stained cells and multiplied by 100.

The percent of active cells of specific taxa was calculated as the number of DAPI stained cells with silver grains and an overlapping signal in the FITC channel (either Bacteria or Thaumarchaeota) divided by the number of DAPI stained cells with an overlapping signal in the FITC channel (either Bacteria or Thaumarchaeota) and multiplied by 100.

(5.2) **Quantitative single cell activity**

The halo area of the silver grains associated with cells (μm^2) obtained in the transmission light mode (tentatively associated to Met or Thy assimilating cells) is a proxy for cell activity.

(I) Single-cell uptake rates were calculated as the silver grain halo area (silver grain halo area measured under the microscope transmission mode) of each cell divided by incubation time in h (μm^2 $cell^{-1}$ h^{-1})

(II) Total uptake rates were estimated as the average of the total silver grain halo area of the two examined filters (Bacteria and Thaumarchaeota) of a specific sample per Liter and per hour (μm^2 L^{-1} h^{-1}). The total silver grain halo area of one filter was calculated according to the following formula:

Total silver grain halo area (μm^2 L^{-1} h^{-1}) = [(Σ silver grain halo area size of all counted cells of the filter / examined area of filter) x total filtered area] / (t x RR x V) x 1000

Where t is the incubation time in h, RR is the ratio of recovery (see below), and V is the sample volume in mL.

The ratio of recovery by MICRO-CARD-FISH of cells from a filter was calculated as follows:

RR = CCm / CCd

Where CCm is the average cell count per field of view obtained with the MICRO-CARD-FISH and CCd is the average cell count per field of view obtained by direct DAPI staining (see below prokaryotic abundance evaluation).

Prokaryotic Abundance. One filter section from each sample was directly stained with DAPI-mix (i.e., neither subjected to click-CARD-FISH nor to MICRO-CARD-FISH protocol) and the cell abundance was microscopically determined. Peeling off the filter-

sections from the slides used in both methods can cause a loss of a fraction of the cells. Thus, the recovery of cells from each sample was calculated after click-CARD-FISH and micro-CARD-FISH protocols and considered to estimate bulk activity of the community (see above).

Results

Environmental conditions. Temperature, salinity and oxygen concentrations throughout the depth profile at both stations are shown in Table S8. Surface chlorophyll-*a* concentrations were higher at station M2 compared to station M4 (Fig. 1).

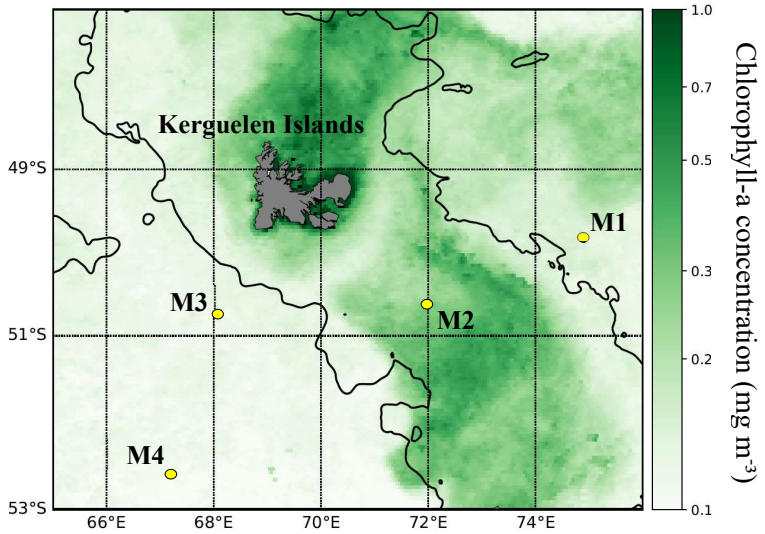

Figure 1. Map of mean surface chlorophyll-a concentrations (mg m^{-3}) in the Southern ocean in March 2018. Data was derived from Global Ocean Satellite Observations (Copernicus-GlobColour), provided from Copernicus Marine Service, and the map was plotted by Stéphane Blain. All sampling stations are depicted (M1 – M4). Resolution: 4 km; bathymetry: black lines indicate 1000 m depth.

Prokaryotic community composition. Both methods, the click-CARD-FISH and the MICRO-CARD-FISH approach, revealed similar results for bacterial and thaumarchaeal abundance (Fig. 2). Generally, Bacteria were more abundant than Thaumarchaeota throughout the water column (Fig. 2). Bacteria contributed 30% – 45% to the total community in epi- and mesopelagic waters and decreased significantly in their contribution to about 20% in the bathypelagic realm. Thaumarchaeota contributed less than 1.5% to the total community in the epipelagic waters. The highest contribution of Thaumarchaeota cells (~10%) to the prokaryotic community was observed in the mesopelagic layer. Towards the bathypelagic realm, Thaumarchaeota represented less than 3.5% of the prokaryotic cells (Fig. 2).

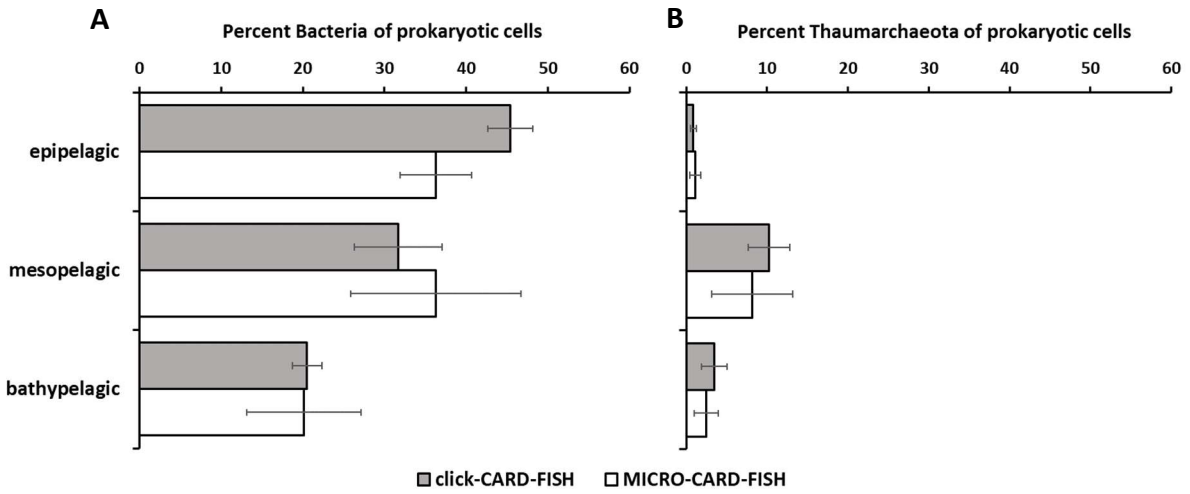

Figure 2. Community composition in the Southern Ocean in different pelagic zones. The percentage of Bacteria (A) and Thaumarchaeota (B) of all DAPI stained cells (total prokaryotic cells) was determined by click-CARD-FISH and MICRO-CARD-FISH. Combined data from stations M2 and M4 are shown (Click-CARD-FISH: epipelagic: n=3, mesopelagic n=7, bathypelagic: n=4; MICRO-CARD-FISH: epipelagic: n=4, mesopelagic: n=6, bathypelagic, n =6). Horizontal bars indicate standard deviation.

Cells taking up substrates. The click-CARD-FISH and the MICRO-CARD-FISH methods revealed similar prokaryotic substrate incorporation trends throughout the water column (Fig. 3). The percentage of cells taking up substrate of all prokaryotic cells did not significantly change with depth at station M2 (ANOVA; n = 12, p = 0.203 for HPG; n = 6, p = 0.078 for Met, p = 0.143 for Thy) (Fig. 3A). At station M4, the percentage of cells taking up these three substrates decreased with depth (Fig. 3B) (ANOVA; n = 16, p = 0.00003 for HPG; n = 10, p = 0.00007 for Met; n = 10, p = 0.02 for Thy). However, the contribution of cells taking up substrates to the prokaryotic cells remained constant below 2500 m depth (ANOVA; n = 6; HPG: p = 0.055, Met: p = 0.093, Thy: p = 0.083) (Fig. 3B).

At Station M2, ~25% of all prokaryotic cells incorporated HPG, whereas ~50% incorporated Met (Fig. 3A). At Station M4, prokaryotes taking up HPG decreased from ~30% of the total prokaryotic cells in the epipelagic to below 10% at near bottom waters. However, 55% and ~17% cells incorporating Met of total prokaryotic cells were detected based on MICRO-CARD-FISH at 100 m depth and near bottom waters, respectively (Fig. 3B). Thus, click-CARD-FISH detected 20 – 30% less cells classified as active cells in epi- and mesopelagic waters than MICRO-CARD-FISH. In the bathypelagic, click-CARD-FISH detected ~ 10% less cells taking up substrate than MICRO-CARD-FISH (Fig. 3).

Thy was generally less incorporated by prokaryotes than Met. About 20% of all prokaryotic cells took up Thy at Station M2 and in epipelagic waters of M4, whereas the percentage decreased to ~10% in the bathypelagic water of Station M4 (Fig. 3).

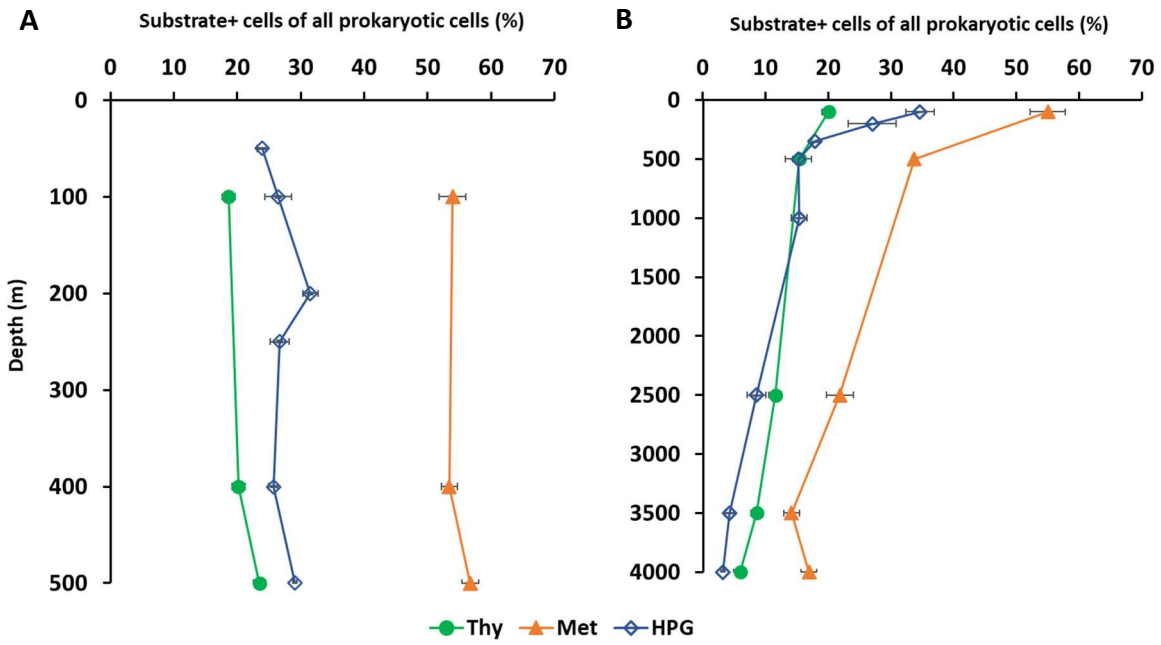

Figure 3. Percentage of HPG, Met and Thy incorporating cells of all prokaryotic cells at different depths of Station M2 (A) and Station M4 (B). Horizontal bars indicate maximum and minimum values.

Single cell activity. Single-cell uptake of Met and Thy (Fig. 4A) and HPG (Fig. 4B) exhibited non-Gaussian distributions in epi- and mesopelagic prokaryotic communities. Met and Thy single-cell uptake assessed by MICRO-CARD-FISH also exhibited a non-Gaussian distribution in the bathypelagic realm (Fig. 4A). In contrast, HPG single-cell uptake determined by click-CARD-FISH showed a more even distribution pattern of the single-cell uptake rates in the bathypelagic waters (Fig. 4B). With increasing depth, the peak of cell counts shifted to smaller single cell activities (Fig. 4).

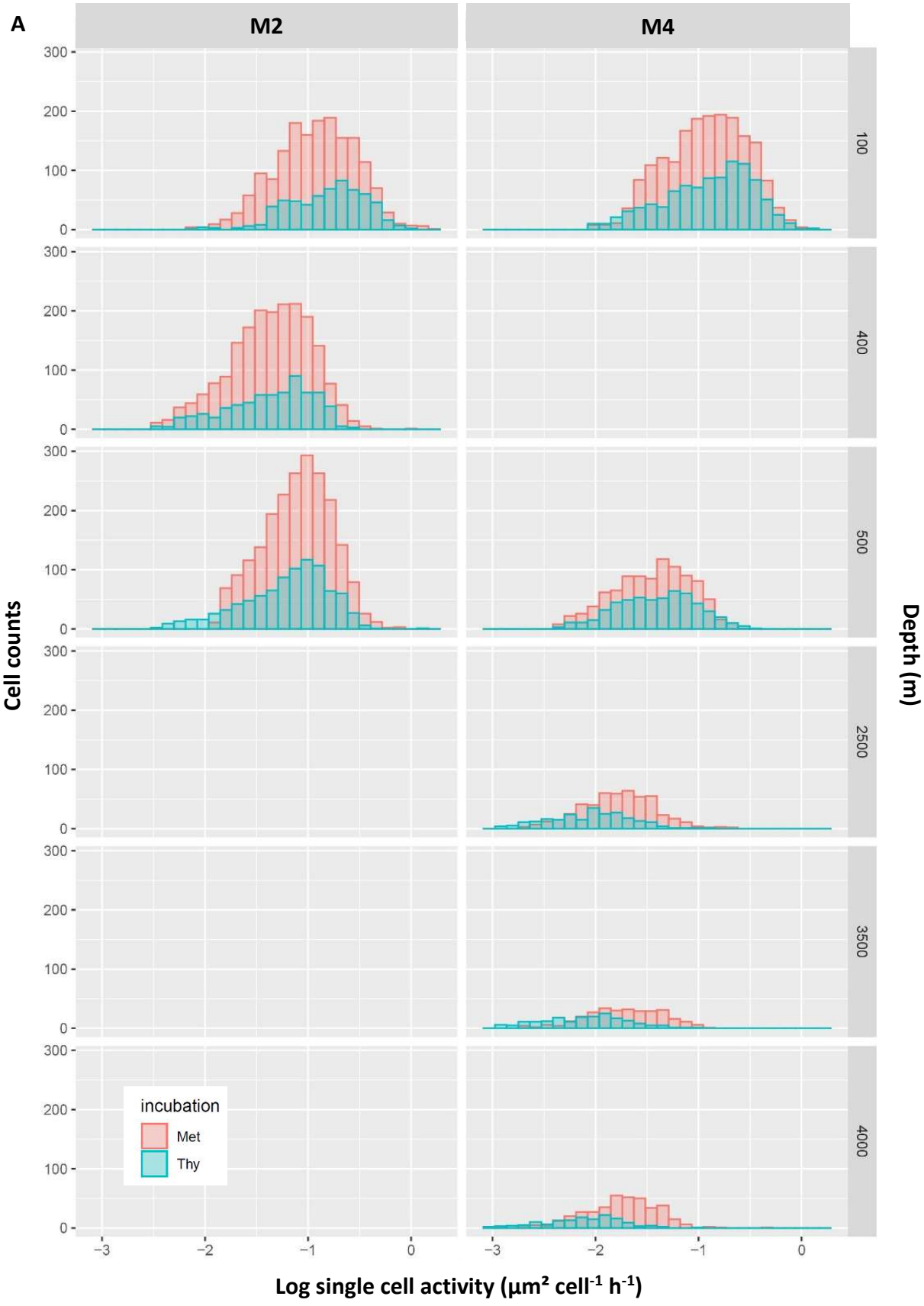
A
M2
M4
100
400
500
2500
3500
4000
Cell counts
Depth (m)
incubation
Met
Thy
Log single cell activity (µm² cell⁻¹ h⁻¹)

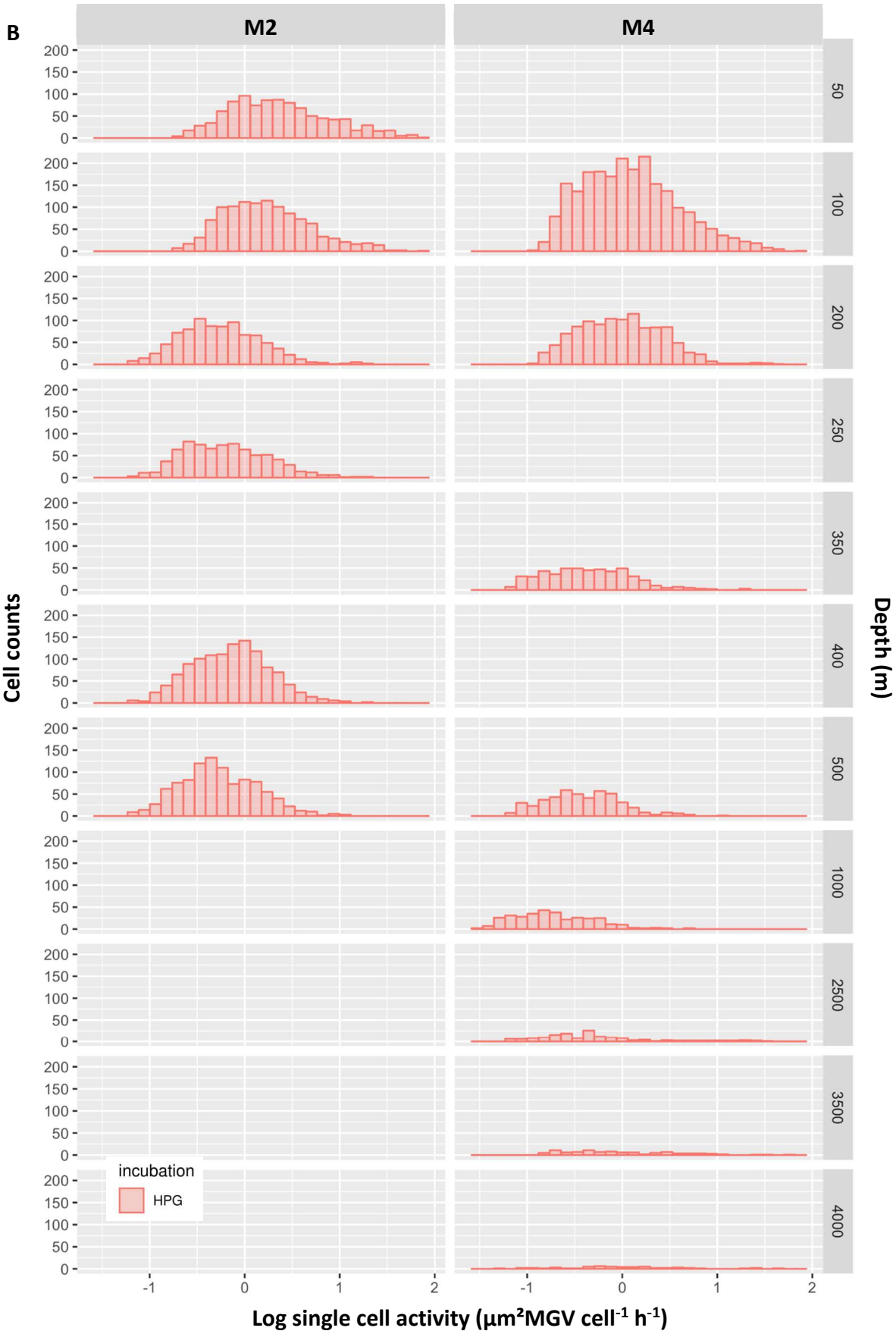

Figure 4. Distribution of single-cell uptake rates at different depths of stations M2 and M4. (A) Methionine and thymidine single cell uptake rates revealed by MICRO-CARD-FISH (µm² cell^{-1} h^{-1}) and (B) HPG single-cell uptake rate assessed by click-CARD-FISH (µm² MGV cell^{-1} h^{-1}).

Relationship between results obtained with click-CARD-FISH and MICRO-CARD-FISH to assess the contribution of active to total cells and total uptake rates. The contribution of active cells to total prokaryotic cells determined by click-CARD-FISH and MICRO-CARD-FISH was linearly correlated (Fig. 5A). However, the contribution of active cells to the prokaryotic cells was higher using MICRO-CARD-FISH than by click-CARD-FISH ($p = 0.012$, $n = 19$, t-test) (Fig. 5A). Total activity rates obtained by both methods were also linearly correlated (Fig. 5B). Total uptake of HPG assessed by click-CARD-FISH and total uptake of Met assessed by MICRO-CARD-FISH exhibited a linear relationship to bulk methionine uptake rate measurements (HPG: $r^2 = 0.98$; Met: $r^2 = 0.96$) (Fig. 6A, B). Total uptake rates of Thy assessed by MICRO-CARD-FISH were also linearly correlated to bulk uptake rate measurements ($r^2 = 0.87$) (Fig. 6C).

Results obtained with MICRO-CARD-FISH showed less variability than click-CARD-FISH, especially for deep-water samples. Technical duplicates were processed to assess the total uptake rate. Coefficient of variance (CV) between duplicates ranged between 1% and 14% for total uptake rates of Met assessed by MICRO-CARD-FISH, whereas CV between duplicates ranged between 2% and 26% in total uptake rates of HPG assessed by click-CARD-FISH until 2500 m depth. Below 2500 m, CV between duplicates in total uptake rates of HPG was > 43%. CV between technical duplicates in total uptake rates of Thy determined by MICRO-CARD-FISH varied between 0% and 11%, except at 500 m depth (CV: 22%) and 4000 m depth (CV: 35%).

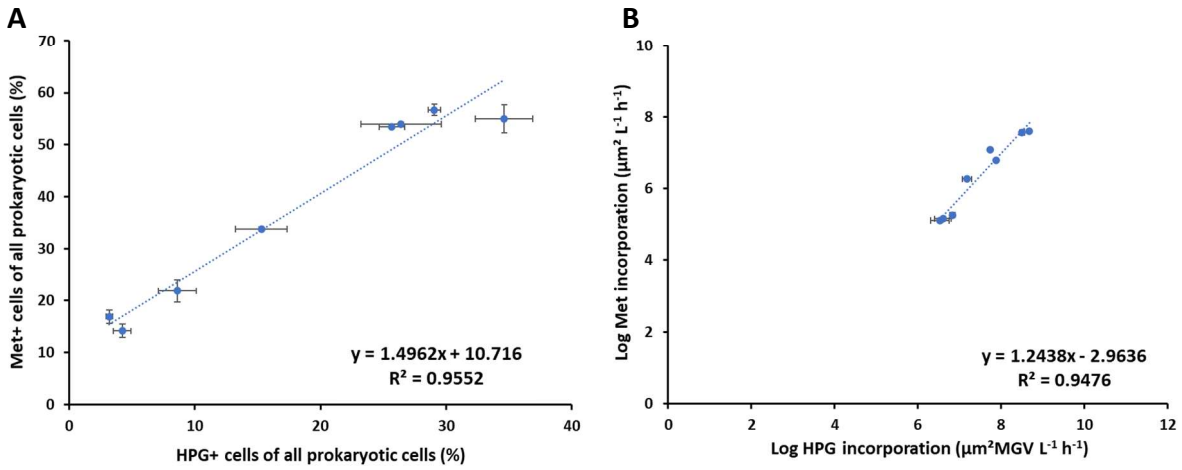

Figure 5. Relationship between click-CARD-FISH and MICRO-CARD-FISH results for (A) contribution of cells taking up Met or HPG of all prokaryotic cells (%) and (B) total activity rates in µm² MGV L^{-1} h^{-1} determined by click-CARD-FISH and µm² L^{-1} h^{-1} determined by MICRO-CARD-FISH. Correlation coefficient (R^2) and regression line function are indicated. Horizontal and vertical bars indicate the maximum and minimum values obtained by click-CARD-FISH and MICRO-CARD-FISH, respectively.

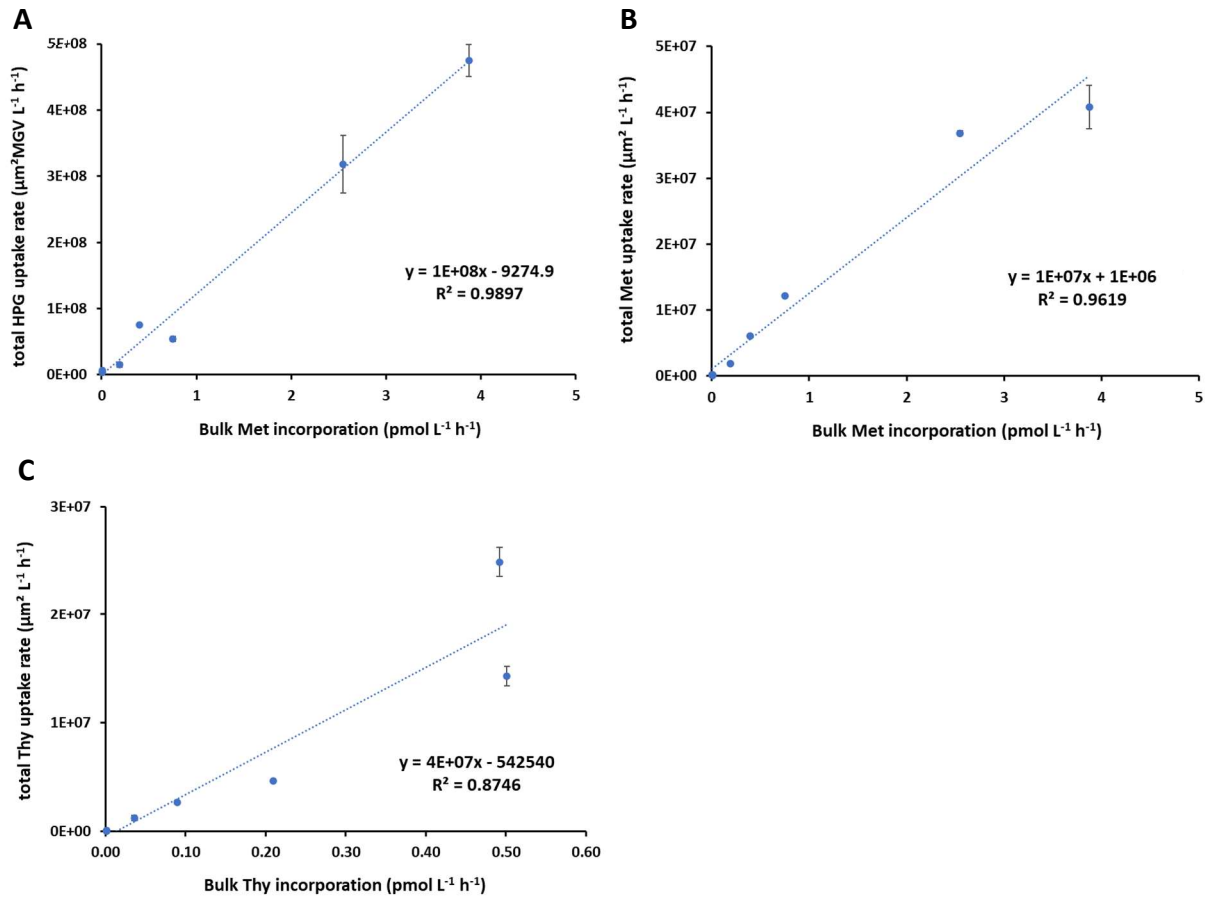

Figure 6. Relationship between the bulk Met and Thy incorporation rates obtained via measuring incorporation rates of the bulk seawater community (pmol L^{-1} h^{-1}) and (A) total uptake rates of HPG determined by click-CARD-FISH (µm²MGV L^{-1} h^{-1}), (B) total uptake rates of Met determined by MICRO-CARD-FISH (µm² L^{-1} h^{-1}), and (C) total uptake rates of Thy determined by MICRO-CARD-FISH (µm² L^{-1} h^{-1}). Correlation coefficient (R^2) and linear equation are indicated. Vertical bars indicate the maximum and minimum values obtained by click-CARD-FISH and MICRO-CARD-FISH.

Distribution of Bacteria and Thaumarchaeota cells taking up HPG, methionine and thymidine. Thaumarchaeota and Bacteria exhibited different substrate uptake patterns. Although Thaumarchaeota exhibited a low relative abundance in epipelagic waters (Fig. 1), up to 75% of all Thaumarchaeota cells incorporated Met and HPG (Fig. 7). Below 100 m depth, the contribution of Thaumarchaeota taking up HPG and Met decreased and remained low throughout the water column and increased slightly in near-bottom waters (Fig. 7A, B). Only a small proportion of all Thaumarchaeota cells were actively taking up Met and HPG in mesopelagic waters (Fig. 7), where they reached highest abundances throughout the water column (Fig. 2). Among the Thaumarchaeota, the contribution of cells taking up Thy did not vary with depth at Station M2 (8.2 ± 2%, mean ± SD, n = 3; 95% confidence interval) and fluctuated but did not significantly differ from their contribution at station M4 (5 - 25%) ($p = 0.085$, n = 8, t-test) (Fig. 8).

The percentage of active bacterial cells taking up HPG, Met or Thy as a fraction of all bacterial cells was rather constant with depth at Station M2, as assessed with MICRO-CARD-FISH (Met: 71 ± 4%, mean ± SD, n= 3; 99% confidence interval [CI]; Thy: 35 ± 2%, mean ± SD, n = 3; 95% CI). A constant contribution of active bacterial cells to the total bacterial cells was also observed from 100 m to 500 m depth as determined by click-CARD-FISH at Station M2 (46 ± 4%, mean ± SD, n = 5; 99% CI) (Figs. 7A, 7B, 8A). At Station M4, the contribution of active bacterial cells to total bacterial cells decreased with increasing depth (Figs. 7C, 7D, 8B).

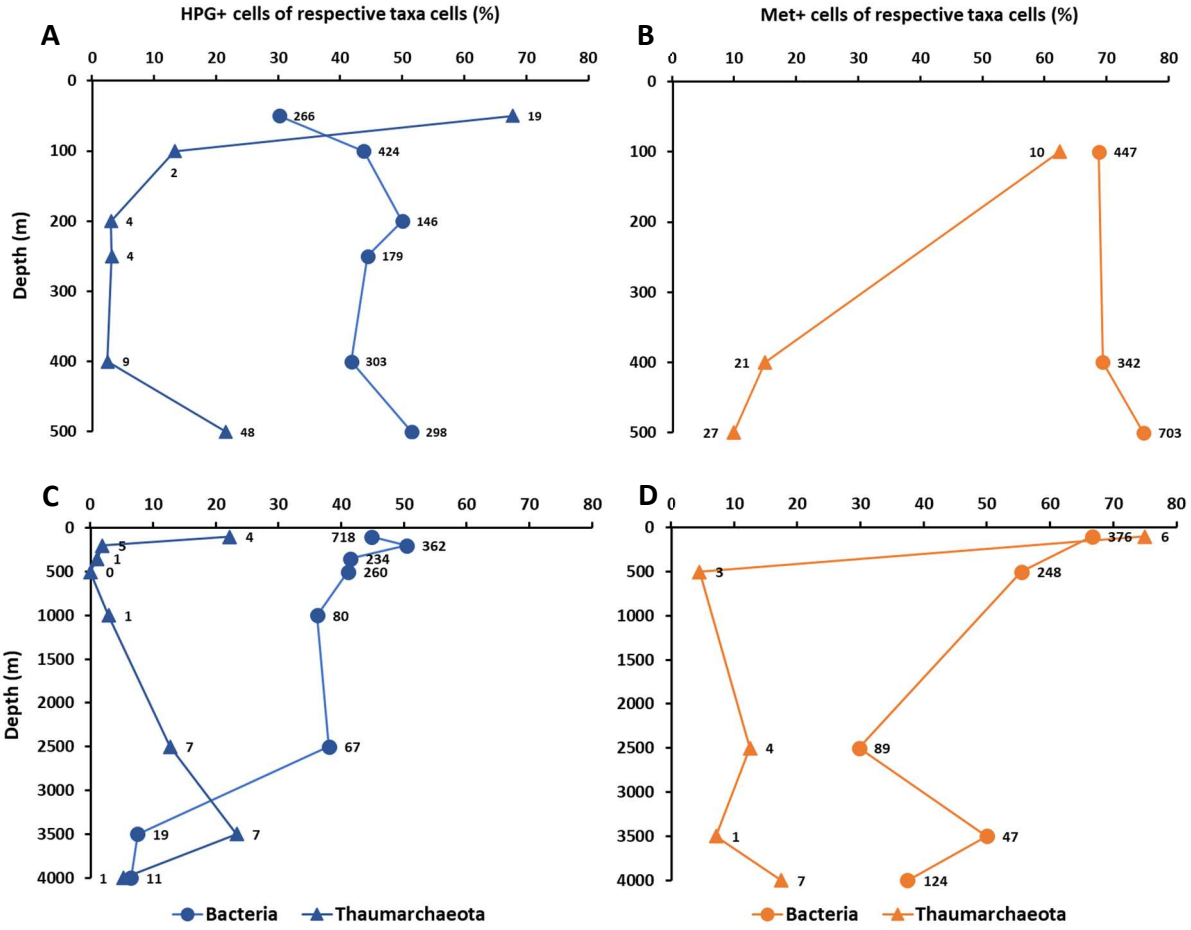

Figure 7. HPG (A, C) and Met (B, D) uptake patterns of Bacteria and Thaumarchaeota throughout the water column in stations M2 (A, B) and M4 (C, D). The percentage of Bacteria taking up HPG or Met of all bacterial cells and of Thaumarchaeota taking up HPG or Met of all thaumarchaeal cells assessed by click-CARD-FISH (HPG, blue) and MICRO-CARD-FISH (Met, orange) are indicated. Numbers next to symbols indicate the number of cells actively taking up the substrate from the respective group microscopically identified per sample and substrate.

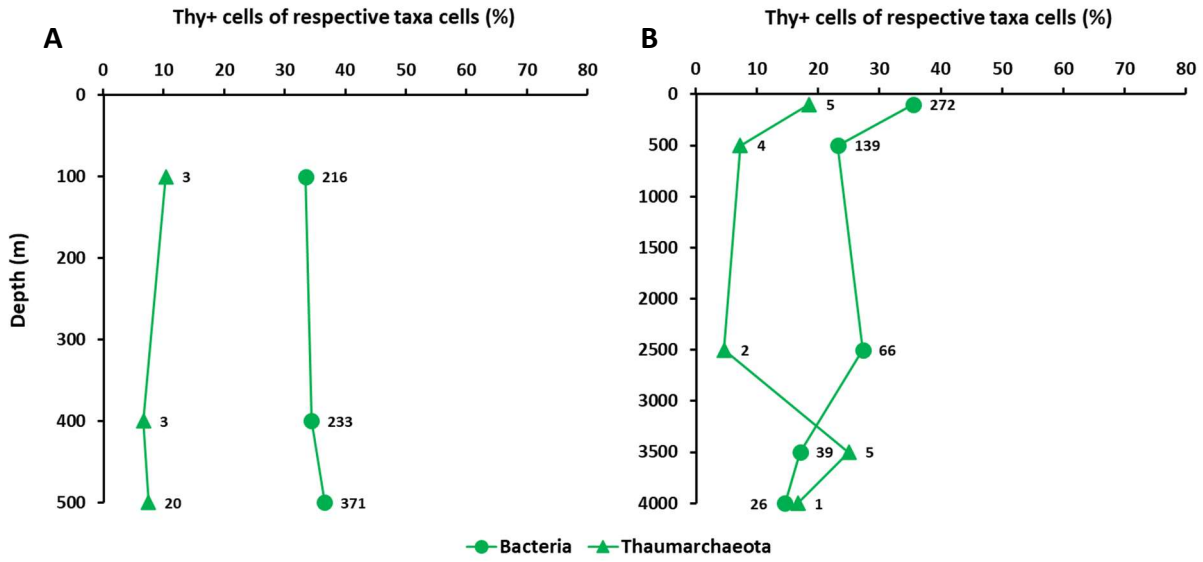

Figure 8. Thy uptake patterns of Bacteria and Thaumarchaeota cells throughout the water column of Station M2 (A) and Station M4 (B). The percentage of Bacteria cells taking up Thy of all bacterial cells and of Thaumarchaeota cells taking up Thy of all thaumarchaeal cells assessed by MICRO-CARD-FISH are indicated. Numbers next to symbols indicate the counts of cells taking up the substrate as microscopically identified per sample.

Single-cell uptake rates of Bacteria and Thaumarchaeota. The single-cell uptake rates of Bacteria exhibited a non-Gaussian distribution for all substrates (HPG, Met, Thy) and depths, linked to the presence of a large fraction of cells with low activity rates. However, the distribution of single-cell uptake rates of HPG at 3500 m and 4000 m were an exception, with an even distribution of cells of different single-cell HPG uptake rates. Thaumarchaeal cells showed a uniform distribution of single cell activity rates throughout the water column at both stations for all substrates (Fig. 9).

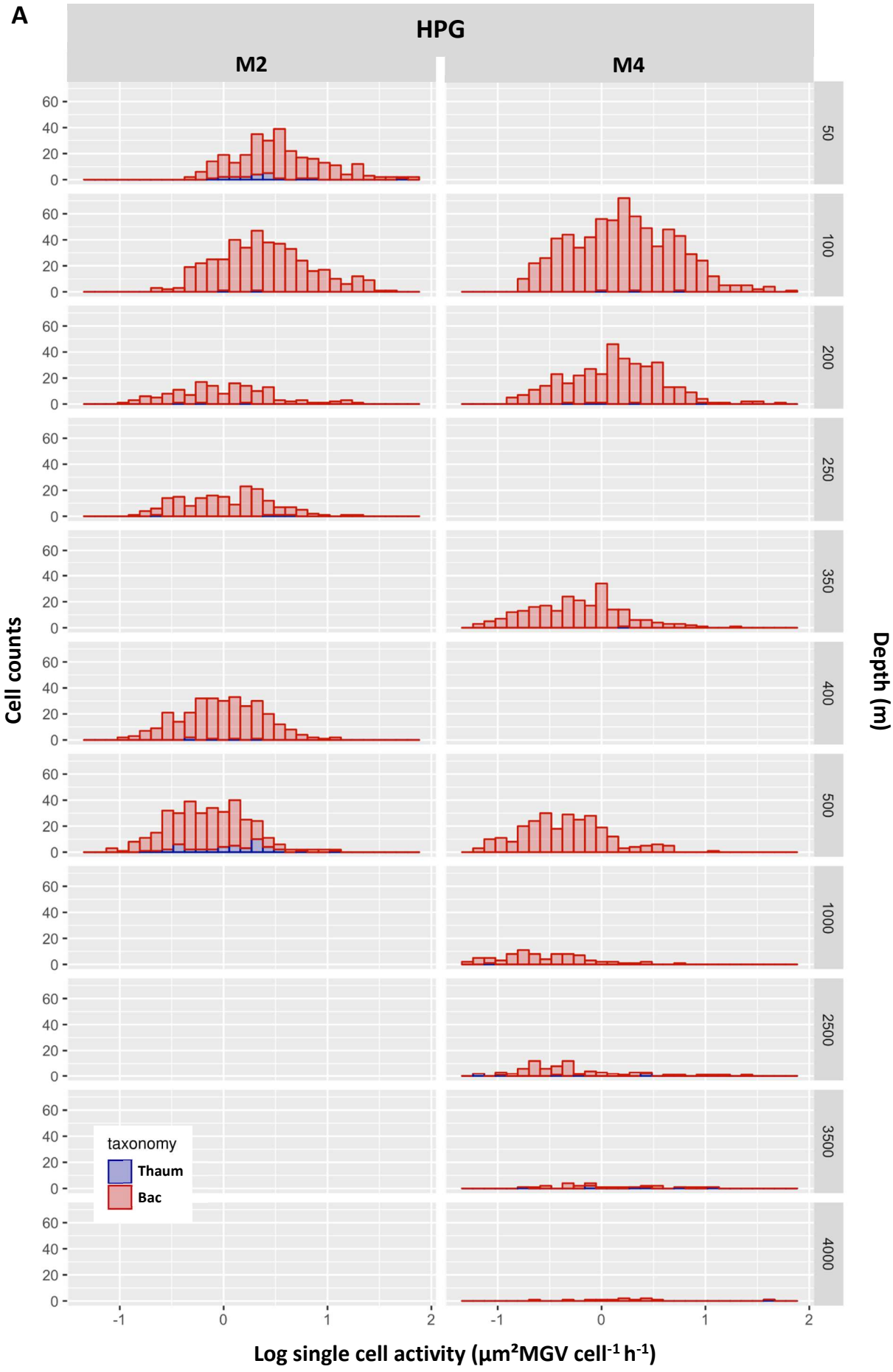
A
HPG
M2
M4
50
100
200
250
350
400
500
1000
2500
3500
4000
Cell counts
Depth (m)
taxonomy
Thaum
Bac
Log single cell activity (µm²MGV cell⁻¹ h⁻¹)

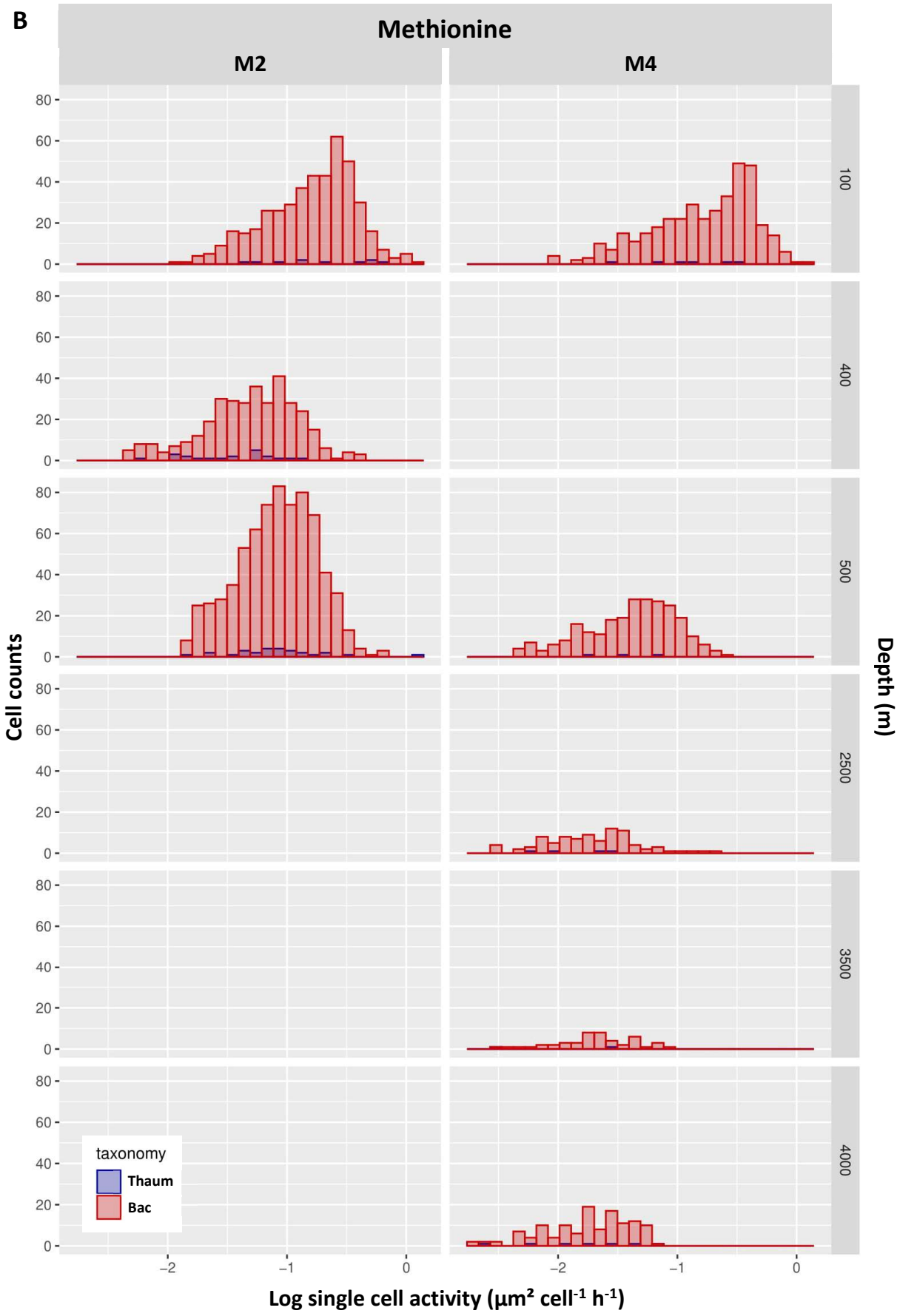
B
Methionine
M2
M4
100
400
500
2500
3500
4000
Cell counts
Depth (m)
taxonomy
Thaum
Bac
Log single cell activity (µm² cell⁻¹ h⁻¹)

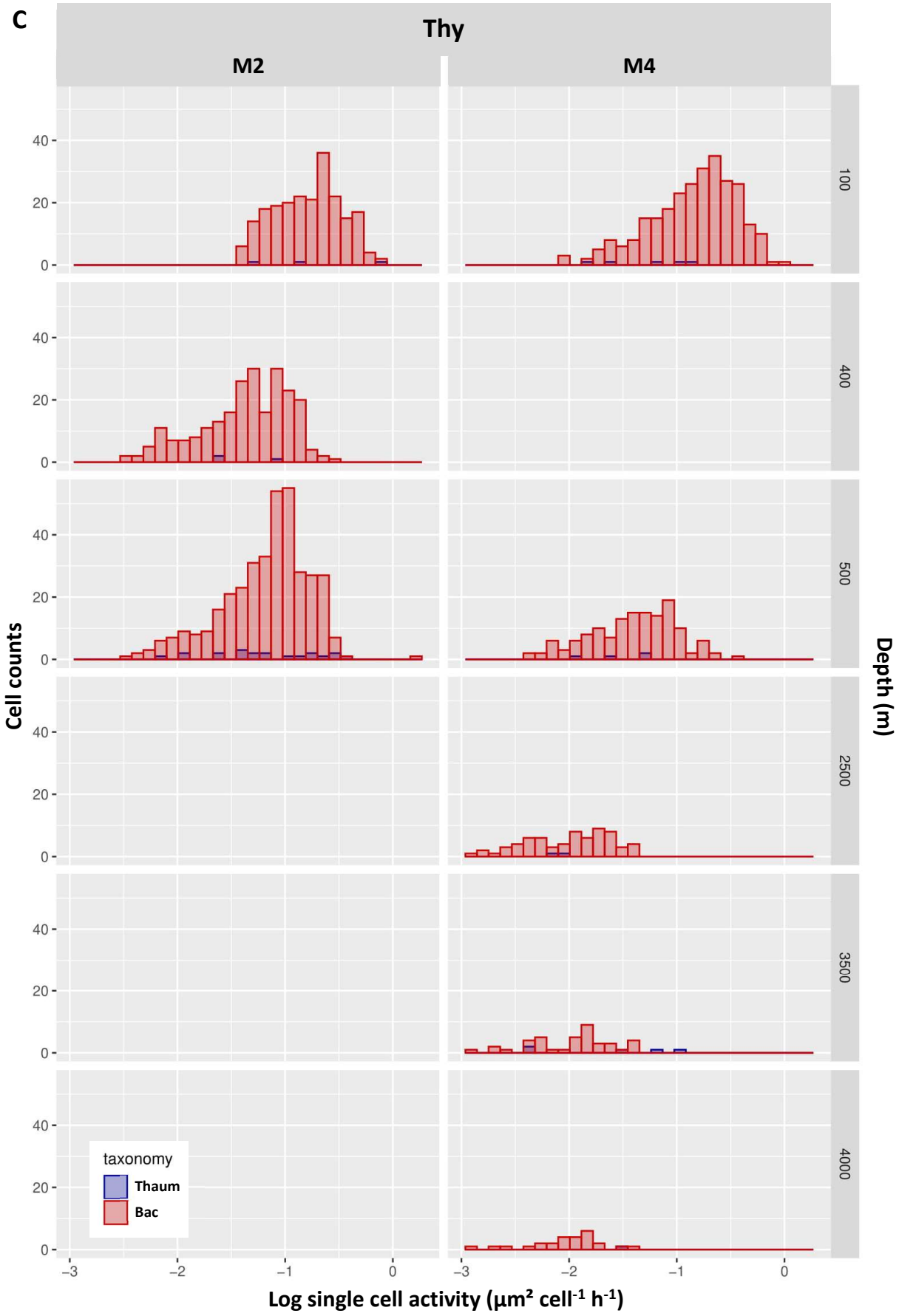

Figure 9. Distribution of bacterial (Bac) and thaumarchaeal (Thaum) single-cell uptake rates of (A) HPG, (B) Met, (C) Thy. Depicted are the cell counts of different areas (a proxy of the activity rate) at each depth of stations M2 and M4.

Contribution of specific taxa to the total prokaryotic cells taking up substrate. Neither the bacterial nor thaumarchaeal contribution to HPG positive cells showed a clear trend with depth (Fig. 10A, B). Bacteria contributed 32% to 77% to the prokaryotic cells taking up HPG, whereas Thaumarchaeota contributed 0% to 12% to the cells taking up HPG.

No significant difference between stations M2 and M4 in the bacterial contribution to Met incorporating cells (t-test p=0.164, n = 8, Fig. 10C, D), and in the bacterial contribution to all Thy incorporating cells (t-test p=0.073, n = 8, Fig. 10E, F) was observed. The bacterial contribution to Met incorporating cells was rather constant at Station M2, ranging from 41% to 64% of all active cells (Fig. 10C) and varied between 29% and 67% at Station M4 (Fig. 10D). Bacteria represented between 53% and 78% of thymidine incorporating cells at Station M2 (Fig. 10E) and 52 ± 5% (mean, SD, n = 5) at Station M4 (Fig. 10F). Thaumarchaeota accounted for a maximum of 5% of all HPG, Met and Thy incorporating cells (Fig. 10).

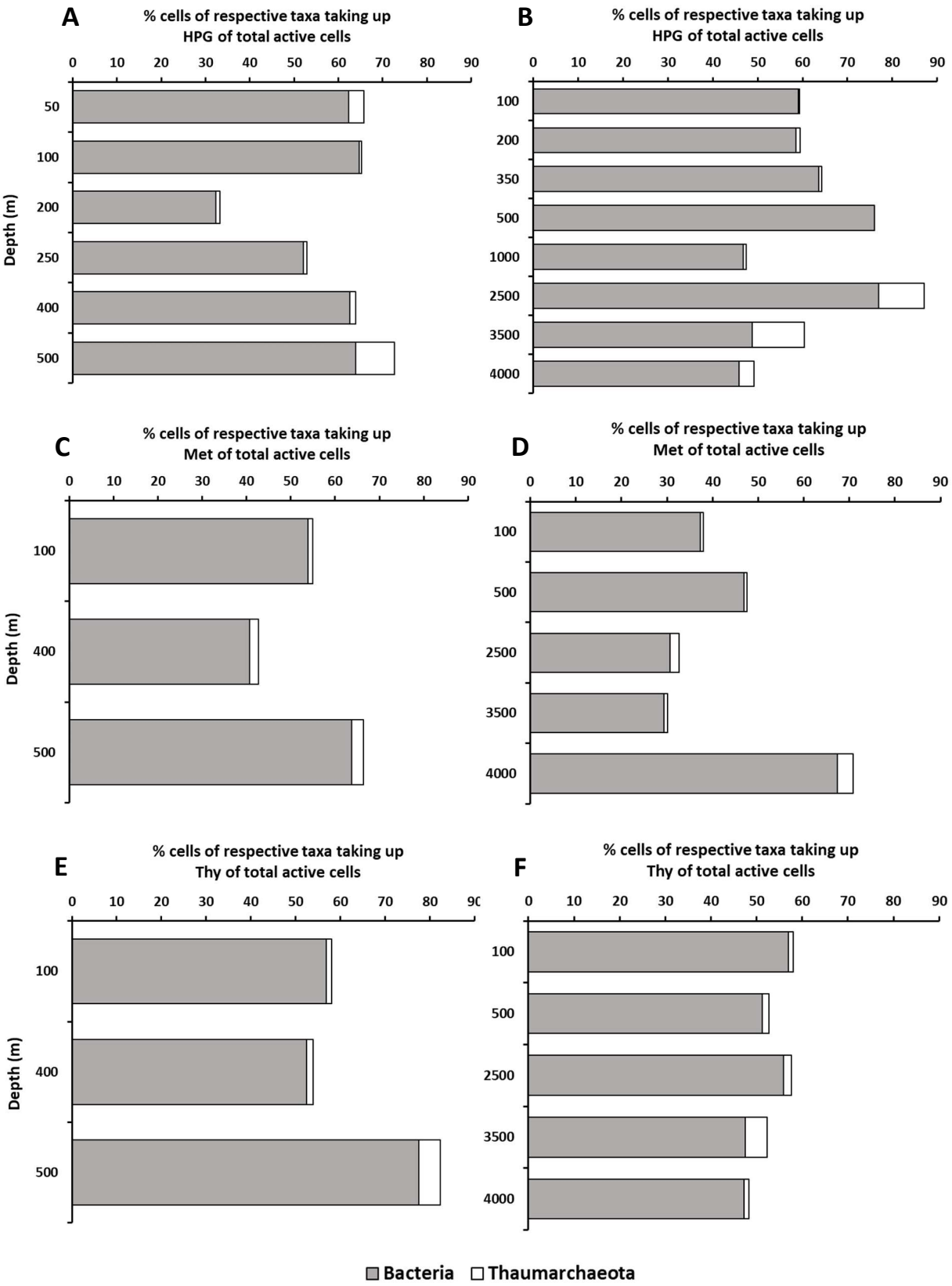

Figure 10. Contribution of Bacteria and Thaumarchaeota cells to the total cells taking up the respective substrate, (A, B) HPG, (C, D) Met and (E, F) Thy at stations M2 (left) and M4 (right).

Discussion

Community Composition. Bacteria exceeded Thaumarchaeota abundance throughout the water column in Antarctic waters close to the Kerguelen Islands (Fig. 2), in agreement with other studies in different oceanic regions, such as the North Atlantic ocean [10, 25, 26, 50], Antarctic ocean [6, 25] and the Pacific gyre [5]. The bacterial contribution to the prokaryotic cell abundance in epi- and mesopelagic waters varying between 30% and 45% (Fig. 2), was comparable to that found in the subtropical North Atlantic gyre, the North Equatorial Counter Current (NEqCC) (~38% – 45%) [10] and the western North Atlantic (~32%) [25, 26, 50].

Thaumarchaeota increased in their contribution to the prokaryotic abundance from epi- to mesopelagic waters (Fig. 2) as shown for other oceanic regions as well [5, 6, 10, 25, 26, 50]. Thaumarchaeal relative abundances of ~2% to ~10% (Fig. 2) were similar to those reported for the subtropical North Atlantic Gyre and the NEqCC [10].

Bacterial and thaumarchaeal relative abundances determined in this study were ~20% and <5 % in the bathypelagic waters, respectively, resulting in ~25% to total DAPI-stained cells. This coverage of the prokaryotic community is much lower than in other studies from the Atlantic [10, 25, 26, 50], Antarctic [6, 25] and Pacific waters [5]. The low coverage in this study might be explained by a low permeabilization efficiency of the prokaryotic cells during the CARD-FISH. Another possibility is low 16S rRNA content of the cells, and consequently less intense fluorescing signals [51]. Prokaryotes in oligotrophic regions generally comprise small, slow growing or dormant cells with low content of r-RNA [52, 53]. However, low productivity or dormant states do not necessarily imply a low number of rRNA [54]. Karner et al. [5] and Varela et al. [10] reported that the sum of bacterial and thaumarchaeal relative abundances in oligotrophic bathypelagic waters (>4000 m depth) were similar to mesopelagic waters (ranging between 40 – 70% of the total prokaryotic cells). Therefore, the low recovery efficiency of prokaryotes with CARD-FISH reported in this study might be due to ineffective permeabilization of the cell wall, preventing large molecules like the HRP to enter the cell [55–58]. Microbial cell wall characteristics are variable; thus, there is no universal permeabilization protocol [56, 58]. The commonly used lysozyme is inefficient to permeabilize gram-positive Bacteria [55, 59] and Archaea [60–63]. Consequently, other protocols using proteinase K [25, 26] or HCL [64, 65] have been developed to permeabilize archaeal cells. Cell wall properties in the bathypelagic realm are influenced by the high pressure and low temperature conditions, causing, e.g., a change in the lipid composition of the membranes [60, 66, 67].

The low fraction of identifiable prokaryotes, not only in the bathypelagic (~25%) but also in epi- and mesopelagic layers (ranging from 37% – 47%), could be partly linked to the

occurrence of some prokaryotic groups not targeted with CARD-FISH in this study, such as Euryarchaeota. Teira et al. [50] stated that Euryarchaea may exhibit larger abundances in colder and recently oxygenated waters. In addition, at 3500 m and 4000 m depth, we detected a large number of very small cell-like and vesicle-like DAPI-stained particles, likely undetected with CARD-FISH.

Comparison between click-CARD-FISH and MICRO-CARD-FISH. Our results indicated ~50% less active cells detected with click-CARD-FISH than with MICRO-CARD-FISH at both stations (M2 and M4) (Fig. 3). In contrast to our results, the previous study comparing microautoradiography and click-chemistry in marine oligotrophic waters [37] suggested that click with HPG yielded a similar or even higher percentage of active cells than microautoradiography with ^{35}S-methionine. These contrasting results could be caused by (I) slight differences in sample processing, such as filter-transfer-freeze technique which resulted in up to 100% active cells in the study of Samo et al. [37], and (II) different sampling location. Regarding the filter-transfer-freeze technique, we found that it strongly diminishes the recovery of cells (cell recovery rate was 3.6 ± 2% (mean, SD, n = 9) for sea surface samples) (Chie Amano, pers. Comm.). Our study was conducted in the open ocean down to 4000 m depth, whereas Samo et al. [37] used oligotrophic coastal marine prokaryotic communities collected at a maximum depth of 60 m, thus comprising more active microbes. However, the most plausible explanation for the contrasting results according to our experience is the dilution of the radioisotope. Samo et al. [37] used 2 nM radiolabeled methionine mixed with 18 nM unlabeled methionine to perform microautoradiography analysis and compared it to 20 nM HPG to perform click analysis. Although dilution of the radiolabeled substrate can be used to evaluate bulk uptake rates of substrates in productive waters, the approach is not applicable to microautoradiography single cell measurements. Bulk uptake rates are evaluated in a volume of seawater (filtered or centrifuged), comprising numerous cells, the total radioactivity is measured and multiplied by the dilution factor of the substrate. However, microautoradiography analysis involves assessing activity of a single cell, and the dilution of the radiolabel strongly decreases the detectability of cells taking up the substrate as cells will develop a smaller or even undetectable silver grain halo, i.e., the dilution cannot be microscopically reverted at a single cell level [27, 68, 69]. Consequently, we used the same concentration of radiolabeled substrate and HPG for a more accurate comparison.

The fluorescing signal resulting from the click method decreases with exposure to light under the epifluorescence microscope, in contrast to the silver grain halo surrounding active

cells under transmission light. Therefore, it is very likely that low activity microbes incorporating less labeled substrate exhibit a weak fluorescing signal and thus, remain undetected using the click-CARD-FISH protocol. Nevertheless, the similar distribution of the single-cell activity (Fig. 4) and the linear relation between (I) the fraction of active cells of the total prokaryotic cells (Fig. 5A), and (II) the total uptake (Fig. 5B) as assessed by click-CARD-FISH and MICRO-CARD-FISH indicates that click-CARD-FISH can be used as a proxy to determine prokaryotic production and single cell activity. However, the results also indicate that until further improvements in detection of low activity cells are achieved, it would be advisable to combine click-CARD-FISH analysis with concurrent bulk radiolabeled substrate uptake rates and MICRO-CARD-FISH analysis.

Single-cell distribution patterns. The distribution of the single-cell activity at stations M2 and M4 (Fig. 4) is consistent with prokaryotic single-cell activity distributions obtained in different oceanic regions, e.g. the Sargasso Sea [70], North Sea [27], Western Arctic ocean [28] and in the Pacific at Scripps pier and off San Diego [37], with a large fraction of cells exhibiting low activity. The low abundance of highly active cells (Fig. 4) can result from the activity of grazers or viral lysis [71, 72], or from non-optimal conditions for the majority of cells [73]. Bacteria exhibit a non-Gaussian distribution of cell uptake rates, whereas Thaumarchaeota show a more even distribution across cell uptake rates (Fig. 9). The difference between taxa-specific cell activity is probably related to the low abundance of Thaumarchaeota cells incorporating the substrates (Fig. 8). Thaumarchaeota are known for amino acid uptake [74], however, Thaumarchaeota are characterized as chemoautotrophs with potential for mixotrophy [75].

Conclusion

Click-CARD-FISH can be used as a proxy for marine prokaryotic production and single-cell substrate incorporation patterns of different taxa of microbial communities. However, it is still necessary to increase the sensitivity of the method to be able to detect low activity cells. Click-CARD-FISH is a relatively inexpensive and fast method to explore different aspects of the physiology of microorganisms, such as the incorporation of specific molecules by specific taxonomic groups or the impact of environmental changes on microbial activity.

References

1. Jan Chrost R, Siuda W. Ecology of Microbial Enzymes in Lake Ecosystems. 2002.

2. Falkowski PG, Fenchel T, Delong EF. The Microbial Engines That Drive Earth's Biogeochemical Cycles. *Science (80-)* 2008; **320**: 1034–1039.

3. Jørgensen BB. Bacteria and Marine Biogeochemistry. *Marine Geochemistry*. 2006. Springer-Verlag, Berlin/Heidelberg, pp 169–206.

4. Simon M, Azam F. Protein content and protein synthesis rates of planktonic marine bacteria. *Mar Ecol Prog Ser* 1989; **51**: 201–213.

5. Karner MB, DeLong EF, Karl DM. Archaeal dominance in the mesopelagic zone of the Pacific Ocean. *Nature* 2001; **409**: 507–510.

6. Church MJ, DeLong EF, Ducklow HW, Karner MB, Preston CM, Karl DM. Abundance and distribution of planktonic Archaea and Bacteria in the waters west of the Antarctic Peninsula. *Limnol Oceanogr* 2003; **48**: 1893–1902.

7. Martiny JBH, Bohannan BJM, Brown JH, Colwell RK, Fuhrman JA, Green JL, et al. Microbial biogeography: putting microorganisms on the map. *Nat Rev Microbiol* 2006; **4**: 102–112.

8. Brown M V., Philip GK, Bunge JA, Smith MC, Bissett A, Lauro FM, et al. Microbial community structure in the North Pacific ocean. *ISME J* 2009; **3**: 1374–1386.

9. Zhou J, Song X, Zhang C-Y, Chen G-F, Lao Y-M, Jin H, et al. Distribution Patterns of Microbial Community Structure Along a 7000-Mile Latitudinal Transect from the Mediterranean Sea Across the Atlantic Ocean to the Brazilian Coastal Sea. *Microb Ecol* 2018; **76**: 592–609.

10. Varela MM, Van Aken HM, Sintes E, Herndl GJ. Latitudinal trends of Crenarchaeota and Bacteria in the meso- and bathypelagic water masses of the Eastern North Atlantic. *Environ Microbiol* 2008; **10**: 110–124.

11. Lechene C, Hillion F, McMahon G, Benson D, Kleinfeld AM, Kampf JP, et al. High-resolution quantitative imaging of mammalian and bacterial cells using stable isotope mass spectrometry. *J Biol* 2006; **5**.

12. Kuypers MMM. Sizing Up the Uncultivated Majority. *Science (80-)* 2007; **317**: 1510–1511.

13. Musat N, Halm H, Winterholler B, Hoppe P, Peduzzi S, Hillion F, et al. A single-cell view on the ecophysiology of anaerobic phototrophic bacteria. *Proc Natl Acad Sci* 2008; **105**: 17861–17866.

14. Musat N, Foster R, Vagner T, Adam B, Kuypers MMM. Detecting metabolic activities in single cells, with emphasis on nanoSIMS. *FEMS Microbiol Rev* 2012; **36**: 486–511.

15. Dekas AE, Poretsky RS, Orphan VJ. Deep-Sea Archaea Fix and Share Nitrogen in Methane-Consuming Microbial Consortia. *Science (80-)* 2009; **326**: 422–426.

16. Orphan VJ, Turk KA, Green AM, House CH. Patterns of 15 N assimilation and growth of methanotrophic ANME-2 archaea and sulfate-reducing bacteria within structured

syntrophic consortia revealed by FISH-SIMS. *Environ Microbiol* 2009; **11**: 1777–1791.

17. Morono Y, Terada T, Nishizawa M, Ito M, Hillion F, Takahata N, et al. Carbon and nitrogen assimilation in deep subseafloor microbial cells. *Proc Natl Acad Sci* 2011; **108**: 18295–18300.

18. Pernice M, Meibom A, Van Den Heuvel A, Kopp C, Domart-Coulon I, Hoegh-Guldberg O, et al. A single-cell view of ammonium assimilation in coral–dinoflagellate symbiosis. *ISME J* 2012; **6**: 1314–1324.

19. Maquelin K, Choo-Smith L-P, Endtz HP, Bruining HA, Puppels GJ. Rapid Identification of Candida Species by Confocal Raman Microspectroscopy. *J Clin Microbiol* 2002; **40**: 594–600.

20. Buijtels PCAM, Willemse-Erix HFM, Petit PLC, Endtz HP, Puppels GJ, Verbrugh HA, et al. Rapid Identification of Mycobacteria by Raman Spectroscopy. *J Clin Microbiol* 2008; **46**: 961–965.

21. Haider S, Wagner M, Schmid MC, Sixt BS, Christian JG, Häcker G, et al. Raman microspectroscopy reveals long-term extracellular activity of chlamydiae. *Mol Microbiol* 2010; **77**: 687–700.

22. Brock TD, Brock ML. Autoradiography as a Tool in Microbial Ecology. *Nature* 1966; **209**: 734–736.

23. Kirchman D, K'nees E, Hodson R. Leucine incorporation and its potential as a measure of protein synthesis by bacteria in natural aquatic systems. *Appl Environ Microbiol* 1985; **49**: 599–607.

24. Kirchman DL. Processes in Microbial Ecology. *Processes in Microbial Ecology* . 2011. Oxford University Press.

25. Herndl GJ, Reinthaler T, Teira E, van Aken H, Veth C, Pernthaler A, et al. Contribution of Archaea to Total Prokaryotic Production in the Deep Atlantic Ocean. *Appl Environ Microbiol* 2005; **71**: 2303–2309.

26. Teira E, Reinthaler T, Pernthaler A, Pernthaler J, Herndl GJ. Combining Catalyzed Reporter Deposition-Fluorescence In Situ Hybridization and Microautoradiography To Detect Substrate Utilization by Bacteria and Archaea in the Deep Ocean. *Appl Environ Microbiol* 2004; **70**: 4411–4414.

27. Sintes E, Herndl GJ. Quantifying Substrate Uptake by Individual Cells of Marine Bacterioplankton by Catalyzed Reporter Deposition Fluorescence In Situ Hybridization Combined with Microautoradiography. *Appl Environ Microbiol* 2006; **72**: 7022–7028.

28. Nikrad MP, Cottrell MT, Kirchman DL. Abundance and Single-Cell Activity of Heterotrophic Bacterial Groups in the Western Arctic Ocean in Summer and Winter. *Appl Environ Microbiol* 2012; **78**: 2402–2409.

29. Cottrell MT, David KL. Contribution of major bacterial groups to bacterial biomass production (thymidine and leucine incorporation) in the Delaware estuary. *Limnol Oceanogr* 2003; **48**: 168–178.

30. Cottrell M, Kirchman D. Single-cell analysis of bacterial growth, cell size, and

community structure in the Delaware estuary. *Aquat Microb Ecol* 2004; **34**: 139–149.

31. DeLong E, Wickham G, Pace N. Phylogenetic stains: ribosomal RNA-based probes for the identification of single cells. *Science (80-)* 1989; **243**: 1360–1363.

32. Amann RI, Krumholz L, Stahl DA. Fluorescent-oligonucleotide probing of whole cells for determinative, phylogenetic, and environmental studies in microbiology. *J Bacteriol* 1990; **172**: 762–770.

33. Pernthaler A, Pernthaler J, Amann R. Fluorescence In Situ Hybridization and Catalyzed Reporter Deposition for the Identification of Marine Bacteria. *Appl Environ Microbiol* 2002; **68**: 3094–3101.

34. Pernthaler A, Preston CM, Pernthaler J, DeLong EF, Amann R. Comparison of Fluorescently Labeled Oligonucleotide and Polynucleotide Probes for the Detection of Pelagic Marine Bacteria and Archaea. *Appl Environ Microbiol* 2002; **68**: 661–667.

35. Leizeaga A, Estrany M, Forn I, Sebastián M. Using Click-Chemistry for Visualizing in Situ Changes of Translational Activity in Planktonic Marine Bacteria. *Front Microbiol* 2017; **8**.

36. Hatzenpichler R, Scheller S, Tavormina PL, Babin BM, Tirrell DA, Orphan VJ. In situ visualization of newly synthesized proteins in environmental microbes using amino acid tagging and click chemistry. *Environ Microbiol* 2014; **16**: 2568–2590.

37. Samo TJ, Smriga S, Malfatti F, Sherwood BP, Azam F. Broad distribution and high proportion of protein synthesis active marine bacteria revealed by click chemistry at the single cell level. *Front Mar Sci* 2014; **1**.

38. Hatzenpichler R, Connon SA, Goudeau D, Malmstrom RR, Woyke T, Orphan VJ. Visualizing in situ translational activity for identifying and sorting slow-growing archaeal−bacterial consortia. *Proc Natl Acad Sci* 2016; **113**: E4069–E4078.

39. Kiick KL, Saxon E, Tirrell DA, Bertozzi CR. Incorporation of azides into recombinant proteins for chemoselective modification by the Staudinger ligation. *Proc Natl Acad Sci* 2002; **99**: 19–24.

40. Dieterich DC, Link AJ, Graumann J, Tirrell DA, Schuman EM. Selective identification of newly synthesized proteins in mammalian cells using bioorthogonal noncanonical amino acid tagging (BONCAT). *Proc Natl Acad Sci* 2006; **103**: 9482–9487.

41. Best MD. Click Chemistry and Bioorthogonal Reactions: Unprecedented Selectivity in the Labeling of Biological Molecules. *Biochemistry* 2009; **48**: 6571–6584.

42. Ngo JT, Tirrell DA. Noncanonical Amino Acids in the Interrogation of Cellular Protein Synthesis. *Acc Chem Res* 2011; **44**: 677–685.

43. van Hest JCM, Kiick KL, Tirrell DA. Efficient Incorporation of Unsaturated Methionine Analogues into Proteins in Vivo. *J Am Chem Soc* 2000; **122**: 1282–1288.

44. Smriga S, Samo T, Malfatti F, Villareal J, Azam F. Individual cell DNA synthesis within natural marine bacterial assemblages as detected by 'click' chemistry. *Aquat Microb Ecol* 2014; **72**: 269–280.

45. Martin JH. Glacial-interglacial CO 2 change: The Iron Hypothesis. *Paleoceanography*

1990; **5**: 1–13.

46. Tagliabue A, Bowie AR, Boyd PW, Buck KN, Johnson KS, Saito MA. The integral role of iron in ocean biogeochemistry. *Nature* 2017; **543**: 51–59.

47. Boyd PW, Jickells T, Law CS, Blain S, Boyle EA, Buesseler KO, et al. Mesoscale Iron Enrichment Experiments 1993-2005: Synthesis and Future Directions. *Science (80-)* 2007; **315**: 612–617.

48. Blain S, Capparos J, Guéneuguès A, Obernosterer I, Oriol L. Distributions and stoichiometry of dissolved nitrogen and phosphorus in the iron-fertilized region near Kerguelen (Southern Ocean). *Biogeosciences* 2015; **12**: 623–635.

49. Daims H, Brühl A, Amann R, Schleifer K-H, Wagner M. The Domain-specific Probe EUB338 is Insufficient for the Detection of all Bacteria: Development and Evaluation of a more Comprehensive Probe Set. *Syst Appl Microbiol* 1999; **22**: 434–444.

50. Teira E, Lebaron P, van Aken H, Herndl GJ. Distribution and activity of Bacteria and Archaea in the deep water masses of the North Atlantic. *Limnol Oceanogr* 2006; **51**: 2131–2144.

51. Hoshino T, Yilmaz LS, Noguera DR, Daims H, Wagner M. Quantification of Target Molecules Needed To Detect Microorganisms by Fluorescence In Situ Hybridization (FISH) and Catalyzed Reporter Deposition-FISH. *Appl Environ Microbiol* 2008; **74**: 5068–5077.

52. Gasol J. Bacteria in oligotrophic environments: Starvation-survival lifestyle. Richard Y. Morita. *Int Microbiol - Off J Spanish Soc Microbiol* 1998.

53. Pernthaler A, Pernthaler J, Schattenhofer M, Amann R. Identification of DNA-Synthesizing Bacterial Cells in Coastal North Sea Plankton. *Appl Environ Microbiol* 2002; **68**: 5728–5736.

54. Blazewicz SJ, Barnard RL, Daly RA, Firestone MK. Evaluating rRNA as an indicator of microbial activity in environmental communities: limitations and uses. *ISME J* 2013; **7**: 2061–2068.

55. Amann RI, Zarda B, Stahl DA, Schleifer KH. Identification of individual prokaryotic cells by using enzyme-labeled, rRNA-targeted oligonucleotide probes. *Appl Environ Microbiol* 1992; **58**: 3007–3011.

56. Schönhuber W, Fuchs B, Juretschko S, Amann R. Improved sensitivity of whole-cell hybridization by the combination of horseradish peroxidase-labeled oligonucleotides and tyramide signal amplification. *Appl Environ Microbiol* 1997; **63**: 3268–3273.

57. Schönhuber W, Zarda B, Eix S, Rippka R, Herdman M, Ludwig W, et al. In Situ Identification of Cyanobacteria with Horseradish Peroxidase-Labeled, rRNA-Targeted Oligonucleotide Probes. *Appl Environ Microbiol* 1999; **65**: 1259–1267.

58. Kubota K. CARD-FISH for Environmental Microorganisms: Technical Advancement and Future Applications. *Microbes Environ* 2013; **28**: 3–12.

59. Sekar R, Pernthaler A, Pernthaler J, Warnecke F, Posch T, Amann R. An Improved Protocol for Quantification of Freshwater Actinobacteria by Fluorescence In Situ Hybridization. *Appl Environ Microbiol* 2003; **69**: 2928–2935.

60. Schleifer KH, Kandler O. Peptidoglycan types of bacterial cell walls and their taxonomic implications. *Bacteriol Rev* 1972; **36**: 407–477.

61. Kandler O, Konig H. Chapter 8 Cell envelopes of archaea: Structure and chemistry. *New Comprehensive Biochemistry*. 1993. pp 223–259.

62. Kandler O, König H. Cell wall polymers in Archaea (Archaebacteria). *Cell Mol Life Sci C* 1998; **54**: 305–308.

63. Kandler O. Cell wall biochemistry in Archaea and its phylogenetic implications. *J Biol Phys* 1995; **20**: 165–169.

64. Molari M, Manini E. Reliability of CARD-FISH Procedure for Enumeration of Archaea in Deep-Sea Surficial Sediments. *Curr Microbiol* 2012; **64**: 242–250.

65. Woebken D, Fuchs BM, Kuypers MMM, Amann R. Potential Interactions of Particle-Associated Anammox Bacteria with Bacterial and Archaeal Partners in the Namibian Upwelling System. *Appl Environ Microbiol* 2007; **73**: 4648–4657.

66. DeLong E, Yayanos A. Adaptation of the membrane lipids of a deep-sea bacterium to changes in hydrostatic pressure. *Science (80-)* 1985; **228**: 1101–1103.

67. Fang J, Chan O, Kato C, Sato T, Peeples T, Nigggemeyer K. Phospholipid FA of piezophilic bacteria from the deep sea. *Lipids* 2003; **38**: 885–887.

68. Nielsen JL, Wagner M, Nielsen PH. Use of Microautoradiography to Study in situ Physiology of Bacteria in Biofilms. *Rev Environ Sci Bio/Technology* 2003; **2**: 261–268.

69. Okabe S, Kindaichi T, Ito T. MAR-FISH—An Ecophysiological Approach to Link Phylogenetic Affiliation and In Situ Metabolic Activity of Microorganisms at a Single-Cell Resolution. *Microbes Environ* 2004; **19**: 83–98.

70. Malmstrom RR, Kiene RP, Cottrell MT, Kirchman DL. Contribution of SAR11 Bacteria to Dissolved Dimethylsulfoniopropionate and Amino Acid Uptake in the North Atlantic Ocean. *Appl Environ Microbiol* 2004; **70**: 4129–4135.

71. Fuhrman JA, Noble RT. Viruses and protists cause similar bacterial mortality in coastal seawater. *Limnol Oceanogr* 1995; **40**: 1236–1242.

72. Pernthaler J. Predation on prokaryotes in the water column and its ecological implications. *Nat Rev Microbiol* 2005; **3**: 537–546.

73. Towbin BD, Korem Y, Bren A, Doron S, Sorek R, Alon U. Optimality and sub-optimality in a bacterial growth law. *Nat Commun* 2017; **8**: 14123.

74. Ouverney CC, Fuhrman JA. Marine Planktonic Archaea Take Up Amino Acids. *Appl Environ Microbiol* 2000; **66**: 4829–4833.

75. Santoro AE, Richter RA, Dupont CL. Planktonic Marine Archaea. *Ann Rev Mar Sci* 2019; **11**: 131–158.

Supplementary information

Table S1. Click-it reaction buffer mix.

Stock reagent	Volume (µl) (in 0.6 ml tube, for ~10 filter section)
Sigma Water	154.4
10x reaction buffer	20
Copper solution	4
Alexa 488 azide	1.6
Buffer additive	20

Table S2. Lysozyme permeabilization mix.

Stock reagent	Volume (µl)	Final
Lysozyme	100 mg	10 mg/ml
1M Tris-HCL	1000	0.1 M
0.5M EDTA	1000	0.5 M
MQ water	8000	

Table S3. Hybridization buffer (HB) mix for Bacteria and Archaea CARD-FISH protocol. Final volume buffer: 300µL; Probe to buffer ratio: 1:20

55% hybridization buffer + HRP probe mix (for Bacteria)		
Stock reagent	**Conc. in stock**	**Volume (µl)**
EUB338I	50 ng/µl of DNA + HRP	1
EUB338II	500 ng/µl of DNA + HRP	1.5
EUB338III	500 ng/µl of DNA + HRP	1.5
55% hybridization buffer		296

55% hybridization buffer		
Stock reagent	**Volume (µL)**	**Final conc.**
5M NaCl	1800	900 mM
1M Tris-HCL	200	20 mM
Dextran Sulfate	1 g	10%
100% Triton X100	5	0.05%
Formamide	5500	55%
10% Blocking	1000	
Sigma Water	1500	

20% hybridization buffer + HRP probe mix (for Archaea)		
Stock reagent	**Conc. in stock**	**Volume (µl)**
CREN 537	50 ng/µl of DNA + HRP	1
CREN 554	50 ng/µl of DNA + HRP	0.5
20% hybridization buffer		298.5

20% hybridization buffer		
Stock reagent	**Volume (µL)**	**Final conc.**
5M NaCl	1800	900 mM
1M Tris-HCL	200	20 mM
Dextran Sulfate	1 g	10%
100% Triton X100	5	0.05%
Formamide	2000	20%
10% Blocking	1000	
Sigma Water	5000	

Table S4. Washing buffer mix for Bacteria and Archaea CARD-FISH protocol.

Washing buffer (for 55 % formamide HB, Bacteria)		
Stock reagent	**Volume (µl)**	**Volume (µl)**
5M NaCl	30	13mM
1M Tris-HCL	1000	20mM
0.5M EDTA	500	5mM
MQ water	48420	
10% SDS	50	0.01%

Washing buffer (for 20 % formamide HB, Archaea)		
Stock reagent	**Volume (µl)**	**Volume (µl)**
5M NaCl	1350	145mM
1M Tris-HCL	1000	20mM
0.5M EDTA	500	5mM
MQ water	47100	
10% SDS	50	0.01%

Table S5. PBS-T mix used for CARD-FISH.

Stock reagent	Volume	Final
1xPBS	50 ml	
100% Triton X100	25 µl	0.05%

Table S6. Amplification Buffer (AMP) used for CARD-FISH combined with click-chemistry or microautoradiography.

Click-CARD-FISH				
solution	**AMP (µl)**	**H_2O_2 (µl)**	**Alexa 555 Tyramide (µl)**	**ratio**
A	200	1 from 30%		
B	493	5 from solution A	5	1:100

AMP for Bacteria with 0.1% blocking reagent, AMP for Archaea with 0.5% blocking reagent. Filters are incubated in solution B.

MICRO-CARD-FISH				
solution	**AMP (µl)**	**H_2O_2 (µl)**	**Alexa 488 Tyramide (µl)**	**ratio**
A	200	1 from 30%		
B	493	5 from solution A	5	1:100

AMP with 0.1% blocking buffer is used for Bacteria and Archaea.
Filters are incubated in solution B.

Amplification buffer (0.1% blocking)		
Stock reagent	**Volume (µL)**	**Final conc.**
Dextran Sulfate	2g	10%
5M NaCl	8000	2 M
10% Blocking	200	0.1%
1x PBS	11800	0.05%

Amplification buffer (0.5% blocking)	
Stock reagent	**Volume (µL)**
AMP (no blocking)	630
10% Blocking	35
1x PBS	35

AMP 0.5% blocking has to be prepared fresh before use.

Amplification buffer (no blocking)		
Stock reagent	**Volume (µL)**	**Final conc.**
Dextran Sulfate	1g	>10%
5M NaCl	4000	>2 M
1x PBS	5000	

Table S7. DAPI-mix used to counterstain the total prokaryotic cells for microscopic assessment.

Stock reagent	**Volume (µl)**	**Final**
DAPI 50 µg/ml	40	2µg/ml
1xPBS	70	0.5
Vectashield	140	1
CitiFluor	750	5.5

Table S8. Temperature (Temp), salinity (Sal) and dissolved oxygen concentration (Oxy) depth profiles at the two stations.

station	depth	Temp. (°C)	Sal	Oxy (µmol/L)
M2	50	5.24	33.86	316.15
	100	2.92	33.91	321.08
	200	1.53	33.97	314.86
	250	1.61	34.06	291.46
	400	2.16	34.30	216.93
	500	2.26	34.40	189.68
M4	100	4.37	33.85	319.21
	200	1.78	33.98	312.33
	350	2.36	34.23	225.95
	500	2.42	34.40	187.33
	1000	2.35	34.68	175.71
	2500	1.15	34.73	202.65
	3500	0.50	34.69	208.15
	4000	0.18	34.68	214.72

Buffers and chemicals

Other chemicals used and preparation of buffers can be found at https://www.microbial-oceanography.eu/methods-instruments/methods/ (2019).

Zusammenfassung

Marine Prokaryoten haben eine Schlüsselrolle in biogeochemischen Kreisläufen. Ein Schlüsselparameter, zur Bestimmung des Beitrages bestimmter prokaryotischer Taxa oder Zellen zu diesen Zyklen und deren ökologische Funktion, ist das Wachstum oder die Aktivitätsrate. Verschiedene Methoden werden angewandt, um die Stoffwechselaktivität und die Biomasse Produktion von individuellen marinen prokaryotischen Zellen zu messen. Mikroautoradiographie wurde in den letzten 20 Jahren in großem Umfang eingesetzt, um die Substratnutzung von marinen Mikrobenzellen nachzuweisen. Kürzlich wurde die „Klick-Chemie“ eingesetzt, um den Einbau fluoreszenzmarkierter Aminosäuren in neu synthetisierten prokaryotischen Proteinen zu detektieren. In dieser Studie haben wir die Anwendbarkeit der Klick-Chemie für Tiefseeproben, unter Verwendung von L-Homopropargylglycin (HPG), einem Methionin-Analog, getestet und mit der Mikroautoradiographie unter Verwendung von Tritium markiertem Methionin verglichen. Zusätzlich wurden die Substrataufnahmeraten von Bakterien und Thaumarchaeota verglichen, indem jede der beiden Methoden mit der „catalyzed reporter deposition fluorescence in situ hybridization“ (CARD-FISH) Methode kombiniert wurde. Bis zu 55% der prokaryotischen Gemeinschaft nahmen Methionin in den epipelagischen Gewässern des Südlichen Ozeans auf. Eine Abnahme der Methionin aufnehmenden Zellen aller prokaryotischen Zellen konnte von 100 m Tiefe auf 500 m Tiefe an der eisenlimitierten Probenstelle beobachtet werden. Im Gegensatz dazu wies der Beitrag der Methionin aufnehmenden Zellen zu allen prokaryotischen Zellen, an der Probenstelle mit natürlich vorkommendem Eisen, keine Unterschiede im Tiefenprofil auf. Unter den prokaryotischen Gruppen trugen Bakterien am meisten zu den Methionin aufnehmenden Zellen bei, während nur wenige Thaumarchaeota Zellen Methionin inkorporierten. Die click-CARD-FISH detektierte weniger aktive Zellen als die MICRO-CARD-FISH. Jedoch zeigen unsere Ergebnisse, dass beide Methoden ähnliche Substratnutzungsmuster der marinen prokaryotischen Gemeinschaft in der gesamten Wassersäule detektieren.